Enhancing gene transfer to renal tubules and podocytes by context-dependent selection of AAV capsids

Taisuke Furusho [1], Ranjan Das [1,7], Hideyuki Hakui [1,7], Anusha Sairavi[1,7], Kei Adachi [1], Mia S. Galbraith-Liss [1], Pratheppa Rajagopal [1], Masahiro Horikawa[2], Shuhua Luo [1], Lena Li[1], Kentaro Yamada [2], Nicole Andeen [3], Gregory A. Dissen[4,5] & Hiroyuki Nakai [1,4,6] ✉

AAV vectors show promise for gene therapy; however, kidney gene transfer remains challenging. Here we conduct a barcode-seq-based comparison of 47 AAV capsids administered through different routes in mice, followed by individual validation. We find that local delivery of AAV-KP1, but not AAV9, via the renal vein or pelvis effectively transduces proximal tubules with minimal off-target liver transduction, while systemic AAV9, but not AAV-KP1, enhances proximal tubule and podocyte transduction in chronic kidney disease. We demonstrate that these contrasting observations are partly due to differences in their pharmacokinetics. Importantly, we show that renal pelvis injection overcomes pre-existing immunity, leading to robust and exclusive proximal tubule transduction, in non-human primates (NHPs). In addition, we highlight drastic differences in renal transduction profiles between mice and NHPs. Thus, this study provides mechanistic insights and underscores importance of context-dependent selection of AAV capsids to overcome challenges in gene delivery to the kidney.

Adeno-associated virus (AAV) vector-mediated in vivo gene therapy has shown success in treating various genetic diseases[1,2]. With recent remarkable progress in the understanding of the genetic etiology of kidney diseases, the success of AAV vector-mediated gene therapy has brought hope to patients affected with genetic kidney diseases, which account for a significant fraction of chronic kidney disease (CKD)[3–5]. However, in contrast to other organs, AAV vector-mediated gene delivery to the kidney remains a challenge. Intravenous (IV) administration of commonly used AAV capsids only achieves mesangial cell and interstitial cell transduction in the kidney[6,7]. Most recent advances have demonstrated podocyte transduction in nephrotic syndrome

mice[8] and the development of an engineered AAV capsid capable of targeting glomerular endothelial cells in rodents[9] following IV administration; however, comprehensive studies on AAV vector-mediated gene delivery to the kidney remains limited, and significant improvements are needed to effectively transduce clinically important cell types, such as tubular epithelial cells and podocytes.

Local administration of AAV vectors, as opposed to their systemic IV delivery, has the potential to enhance target tissue transduction and prevent off-target effects. For renal gene transfer, renal vein (RV) injection, and renal pelvis (RP) injection are the two common local routes of administration that have been studied[10–14]. Although some

[1]Department of Molecular and Medical Genetics, Oregon Health & Science University School of Medicine, Portland, OR, USA. [2]Dotter Department of Interventional Radiology, Oregon Health & Science University School of Medicine, Portland, OR, USA. [3]Department of Pathology, Oregon Health & Science University School of Medicine, Portland, OR, USA. [4]Division of Neuroscience, Oregon National Primate Research Center, Oregon Health & Science University, Beaverton, OR, USA. [5]Molecular Virology Core, Oregon National Primate Research Center, Oregon Health & Science University, Beaverton, OR, USA. [6]Department of Molecular Microbiology and Immunology, Oregon Health & Science University School of Medicine, Portland, OR, USA. [7]These authors contributed equally: Ranjan Das, Hideyuki Hakui, Anusha Sairavi. ✉e-mail: nakaih@ohsu.edu

studies compared the renal transduction efficiencies of common AAV capsids[6,10–12], the impact of the administration route on the renal transduction profiles of various AAV capsids remains poorly understood. Regarding off-target effects, minimizing vector dissemination to off-target organs is important to prevent serious side effects, including hepatotoxicity, genotoxicity, thrombotic microangiopathy, and dorsal root ganglia (DRG) toxicity[1,2,15]. However, recent studies have shown off-target liver transduction by AAV8 and AAV9 following RV[10] and RP[11] injections, indicating that these commonly used AAV capsids are not ideal for local injection. It has yet to be determined which AAV capsids are suitable for local kidney injection while minimizing off-target effects. In addition, how renal transduction profiles, determined by AAV capsids and routes of administration, vary across different species and the mechanisms driving these differences, are largely unknown. Moreover, renal transduction profiles in CKD have yet to be established.

In this study, we assessed renal transduction efficiencies of various AAV capsids in mice by IV, RV, and RP injections using AAV Barcode-Seq[16], followed by individual capsid validation in mice and non-human primates (NHPs). Six capsids, including AAV-KP1[17], showed remarkably enhanced renal transduction via RV and RP routes in mice, and RP injection overcame pre-existing anti-AAV neutralizing antibodies (NAbs) in NHPs. The study also revealed marked differences in renal transduction profiles between healthy and CKD kidneys and distinct renal transduction pathways in mice and NHPs. These observations emphasize the importance of the optimal selection of both the AAV capsid and the route of administration, considering the host and its disease conditions.

Results

Barcode-Seq of 47 AAVs for renal transduction in mice

We first investigated which AAV capsids transduce the kidney most efficiently by IV, RV, and RP injections in mice using AAV Barcode-Seq[16,18] (Fig. 1a). The design allows the assessment of relative transduction efficiency at both DNA and RNA levels (*i.e.*, DNA/RNA Barcode-Seq). We produced an AAV barcode library that contained 47 AAV capsids (20 naturally occurring serotypes and 27 capsid-engineered mutants, Supplementary Table 1) and injected the library via IV (2.0×10^{13} vg/kg), RV (3.0×10^{11} vg/mouse) or RP (3.0×10^{11} vg/mouse) into 8-week-old C57BL/6 J male mice ($n = 3$ for IV and RP, $n = 4$ for RV). RV and RP injections were performed with the blockade of the local renal blood flow for 15 min based on previously reported methods[10,14] to increase vector exposure. Urinary flow was also blocked for RP injection. Six weeks post-injection, the transduction efficiency of each AAV capsid in the kidney relative to that of AAV9 was determined by AAV DNA/RNA Barcode-Seq. We found that (a) no capsid transduced the kidney more efficiently than AAV9 by IV injection; (b) by RV and RP injections, AAV-KP1, AAV-KP2, AAV-KP3[17], AAV-DJ[19], AAV2G9[20] and AAV2.7m8[21] showed higher renal transduction than AAV9 at the level of vector genome mRNA transcripts with statistical significance; (c) there was a DNA-RNA correlation for these six AAV capsids; (d) AAV3, AAV-LK03 and AAVShH10 exhibited significantly enhanced DNA delivery to the kidney while mediating transgene expression at significantly lower levels compared to AAV9 following RV or RP injection (Fig. 1b and Supplementary Fig. 1 and see Supplementary Discussion 1).

Efficient proximal tubule transduction by local injection of AAV-KP1

To validate the AAV Barcode-Seq data, we individually packaged the AAV-CAG-tdTomato genome with AAV9 and AAV-KP1 capsids and produced AAV9-CAG-tdTomato and AAV-KP1-CAG-tdTomato vectors. Each of the two vectors was injected into 8-week-old C57BL/6 J male mice by IV, RV or RP injection at a dose of 3.0×10^{11} vg/mouse ($n = 4$ per group, Fig. 2a). We selected AAV-KP1 from the six AAV capsids showing the enhancement as it was one of the most efficient capsids for kidney transduction by both RV and RP injections based on the AAV Barcode-

Seq data. Two weeks post-injection, vector genome copy numbers in the kidney were determined by DNA qPCR and renal transduction was assessed by fluorescence microscopy. Quantification of vector genomes in the kidney showed that vector genome copy numbers were comparable between the AAV9-injected and AAV-KP1-injected mice in the IV group, while there were 35 times and 23 times more vector genomes in the AAV-KP1-injected mice than the AAV9-injected mice following RV and RP injections, respectively (Fig. 2b). Vector genome copy numbers in the AAV9-injected animals were not different between the IV, RV and RP groups, demonstrating that there is no advantage of local administration over systemic administration when AAV9 capsid is used. Consistent with the vector genome copy number data, the histological assessment showed enhanced transduction in the kidney with AAV-KP1 following RV and RP injections compared to IV injection (Fig. 2c).

Interestingly, reciprocal transduction levels of AAV9 and AAV-KP1 were observed in the kidney and liver following RV and RP injections. Quantification of vector genomes in the liver two weeks after IV, RV and RP injections revealed that both AAV9 and AAV-KP1 are equally liver tropic by IV injection, while RV and RP injections of the AAV-KP1 reduced the off-target liver transduction by 14-fold and 7-fold compared to IV injection, respectively (two-way ANOVA followed by Tukey's post hoc test, adjusted $p = 5.8 \times 10^{-6}$ and 6.7×10^{-4} for RV and RP). On the other hand, off-target liver transduction was not prevented by RV and RP injections of AAV9 (Fig. 2b). A fluorescence microscopic analysis also confirmed suppressed off-target liver transduction by RV and RP injections of AAV-KP1 compared to AAV9 (Fig. 2d).

Next, we assessed which cell types in the kidney were transduced by local injection of AAV-KP1. Co-staining with Lotus tetragonolobus lectin (LTL, a proximal tubule marker) revealed that enhanced transduction of AAV-KP1 was mainly observed in the cortex, specifically the proximal tubules (Fig. 3a). The proximal tubule transduction was 9.9% and 8.7% by RV and RP injections of AAV-KP1, respectively (Fig. 3c), whereas AAV-KP1 transduced only mesangial cells in the glomeruli by IV injection (Fig. 3a and Supplementary Fig. 2a). Additional transduction was observed in parietal cells (Supplementary Fig. 2c), collecting duct cells (Supplementary Fig. 2e), and interstitial cells (indicated by arrows in Fig. 3a) by local injection of AAV-KP1. AAV9 transduced mesangial cells, interstitial cells, and thick ascending limb cells adjacent to the juxtaglomerular apparatus as previously reported[6], which remained unaltered irrespective of the administration route (Supplementary Fig. 2). No appreciable transduction in podocytes was observed with AAV9 or AAV-KP1 regardless of the administration routes (Fig. 3b). Efficient proximal tubule transduction with AAV-KP1 following RV and RP injections was reproducible in female mice (Supplementary Fig. 3).

Ischemia does not enhance renal transduction of AAV-KP1

Since we performed RV and RP injections with the 15-minute blockade of the local arterial and venous flow, we investigated if ischemia influences renal transduction. We found that IV injection of AAV-KP1-CAG-tdTomato (3.0×10^{11} vg/mouse) into 8-week-old C57BL/6 J male mice following 15 min renal ischemia did not alter the transduction, showing only mesangial cell transduction (Supplementary Fig. 4a, b). This indicates that ischemia is not the cause of enhanced renal transduction achieved by RV or RP injection. We also performed RV and RP injections of AAV-KP1-CAG-tdTomato (3.0×10^{11} vg/mouse) with varying ischemic time periods from 0 min up to 15 min (Supplementary Fig. 4c). There was no apparent difference in transduction efficiency by RV between the following four ischemic time periods (< 1, 5, 10 and 15 min). In the RP injection group, while there was no difference in transduction efficiency between the 5, 10, and 15-min time period groups, RP injection without blockade of the renal artery and vein blood flow resulted in
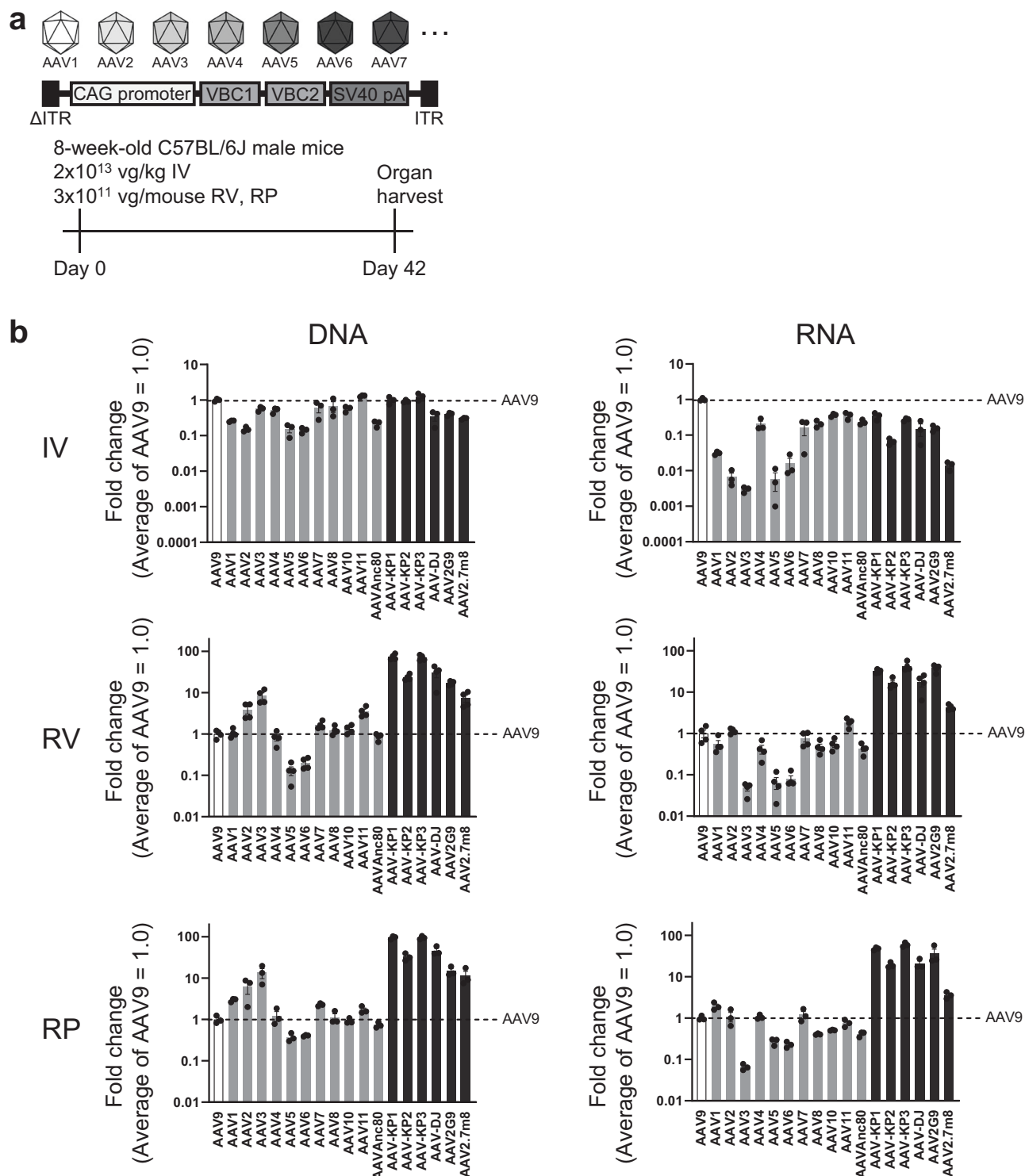
Fig. 1 | AAV Barcode-Seq analysis of AAV capsids for renal transduction following IV, RV, and RP injections. a The experimental design. Eight-week-old C57BL/6J male mice were injected with an AAV-CAG-VBC barcode library that contained 47 AAV capsids via IV (2.0×10^{13} vg/kg), RV (3.0×10^{11} vg/mouse) or RP (3.0×10^{11} vg/mouse) injection. $N = 3$ for IV and RP, and $n = 4$ for RV. Kidneys were harvested 6 weeks post-injection for the AAV Barcode-Seq analysis. **b** Relative quantities of each AAV capsid-derived vector genome (DNA) and vector genome transcript (RNA) in the kidney were determined by AAV Barcode-Seq and expressed as fold changes using AAV9 as the benchmark. The light bars represent common AAV serotypes. The dark bars represent the six AAV capsids showing significantly enhanced transduction compared to AAV9. Data are presented as mean ± standard error of the mean. A one-way ANOVA followed by Tukey's post hoc test was used for statistical assessment of the data. Adjusted $p < 0.05$ was considered statistically significant. The 29 AAV capsids that are not included in this figure are: AAVbb.2, AAVhu.11, AAVhu.13, AAVhu.37, AAVpo1, AAVrh.8, AAVrh.10, AAVrh.20, AAVrh.43, AAV1.9mt100, AAV1.9mt30, AAV1.9mt76, AAV2i8, AAV2retro, AAV2R585E, AAV2R585E9.2, AAV9AA272, AAV9AA22, AAV9W22A, AAV-HN1, AAV-HN2, AAV-HN3, AAV-LK03, AAV-NP40, AAV-NP59, AAVPHP.B, AAVPHP.eB, AAVPHP.S, AAVShH10. For the complete information on the 47 AAV capsids, refer to Supplementary Fig. 1. Source data and exact p values are provided in the Source Data file.
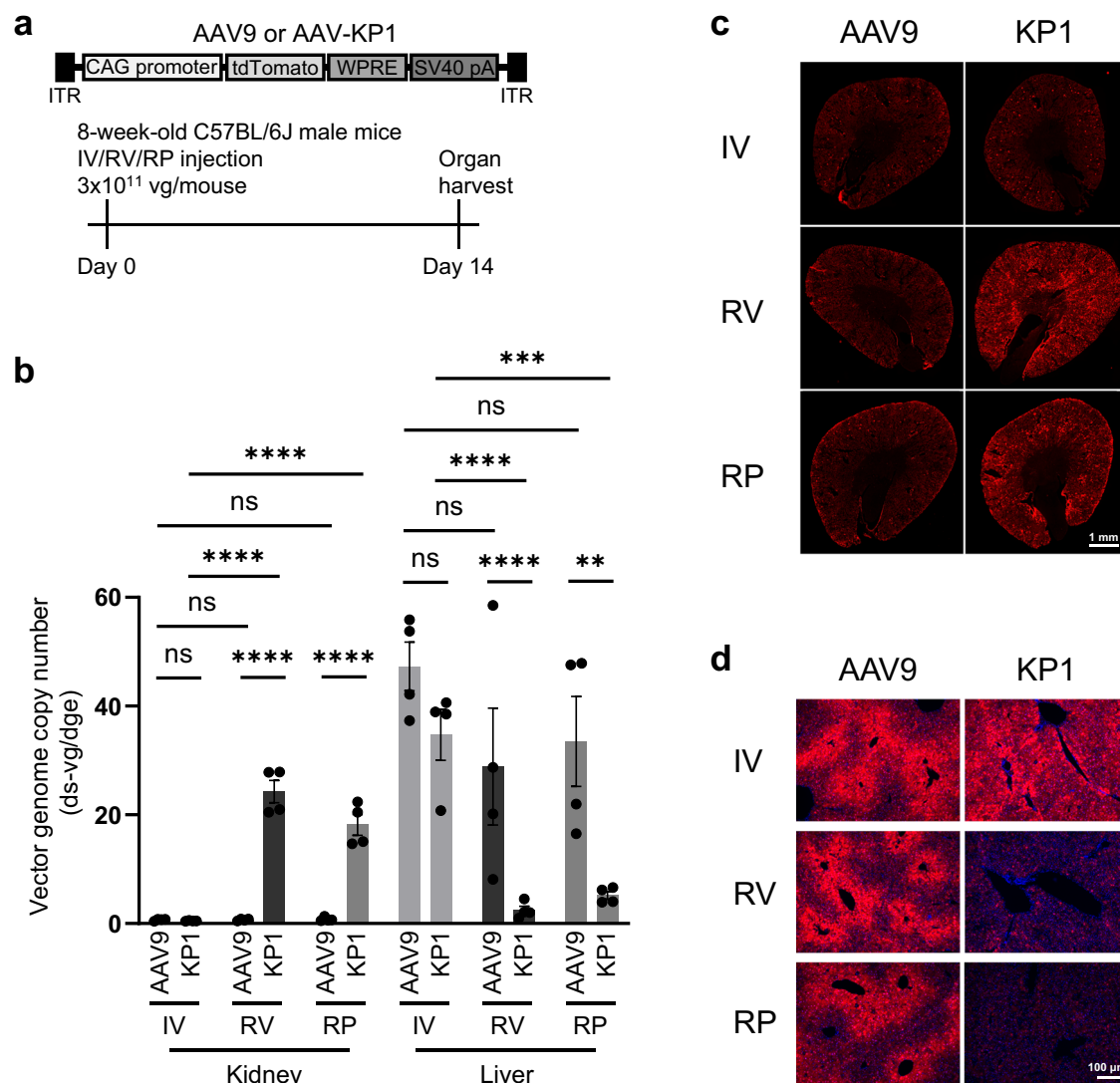
Fig. 2 | Enhanced renal transduction and reduced off-target liver transduction with AAV-KP1 by RV or RP injection. a The experimental design. Eight-week-old C57BL/6J male mice were injected with AAV9-CAG-tdTomato or AAV-KP1-CAG-tdTomato via IV, RV, or RP injection at a dose of 3.0×10^{11} vg/mouse ($n = 4$ per group). Kidneys and livers were harvested 2 weeks post-injection for downstream analyses. **b** AAV vector genome copy numbers in the kidneys and livers determined by qPCR. Each data point corresponds to a different mouse. Vector genome copy numbers are expressed as double-stranded (ds) vector genome copy numbers per diploid genomic equivalent (ds-vg/dge). A two-way ANOVA followed by Tukey's post hoc test was used for statistical assessment of the data. ****, adjusted $p < 0.0001$; ***, adjusted $p < 0.001$; **, adjusted $p < 0.01$, ns, not significant. Data are presented as mean ± standard error of the mean. **c** Representative images of native tdTomato fluorescence in the kidney. Please note that, for the RV and RP groups, the data obtained from the AAV vector-treated kidneys, not non-treated kidneys in the same animals, are presented. Scale bar indicates 1 mm. **d** Representative fluorescence microscopic images of the livers in the AAV vector-treated mice. Red, native tdTomato fluorescence; blue, DAPI. The scale bar indicates 100 μm. Source data and exact p-values are provided in the Source Data file.

lower transduction than that in the other groups, showing no proximal tubule transduction (Supplementary Fig. 4d). These observations suggest that prolonged ischemia does not confer any benefits to kidney cell transduction while the blockade of the renal blood flow at the time of injection is a crucial step for RP injection to mediate effective renal transduction in mice.

Vector accumulates in interstitium by local injection in mice
When AAV vectors are administered intravascularly, vascular endothelial cells pose a significant physical and functional barrier for in vivo AAV vector transduction in the organs whose endothelium is devoid of fenestrae (*i.e.*, continuous endothelium) such as the brain, heart, and skeletal muscles[22]. In the kidney, endothelial cells of cortical peritubular capillaries and glomeruli are both fenestrated by holes of ~ 60–80 nm in diameter, with the former having a diaphragm and the latter being devoid of it[23]. In addition, there is no basement membrane

between the glomerular endothelial cells and the mesangial interstitial space in contrast to the peritubular capillary and the other renal blood vessels that have a basement membrane[24,25]. Based on these micro-anatomical structures of the kidney, we reasoned that the mesangial interstitial space is more accessible by intravascularly injected AAV than the peritubular interstitium.

To investigate the mechanism of enhanced transduction by RV and RP injections in mice, we assessed the distribution and extravasation of AAV in the kidney following AAV vector injection by IV, RV, and RP. To this end, we employed fluorescent microspheres of 25 nm in diameter to mimic AAV. After 30 min circulation, microspheres administered intravenously mainly accumulated in the mesangial area of the glomeruli (Supplementary Fig. 5a, b), consistent with the previous findings that nanoparticles accumulate in the mesangial area in a size-dependent manner[26,27]. This observation is in line with our knowledge of the above-described anatomical structure of the kidney
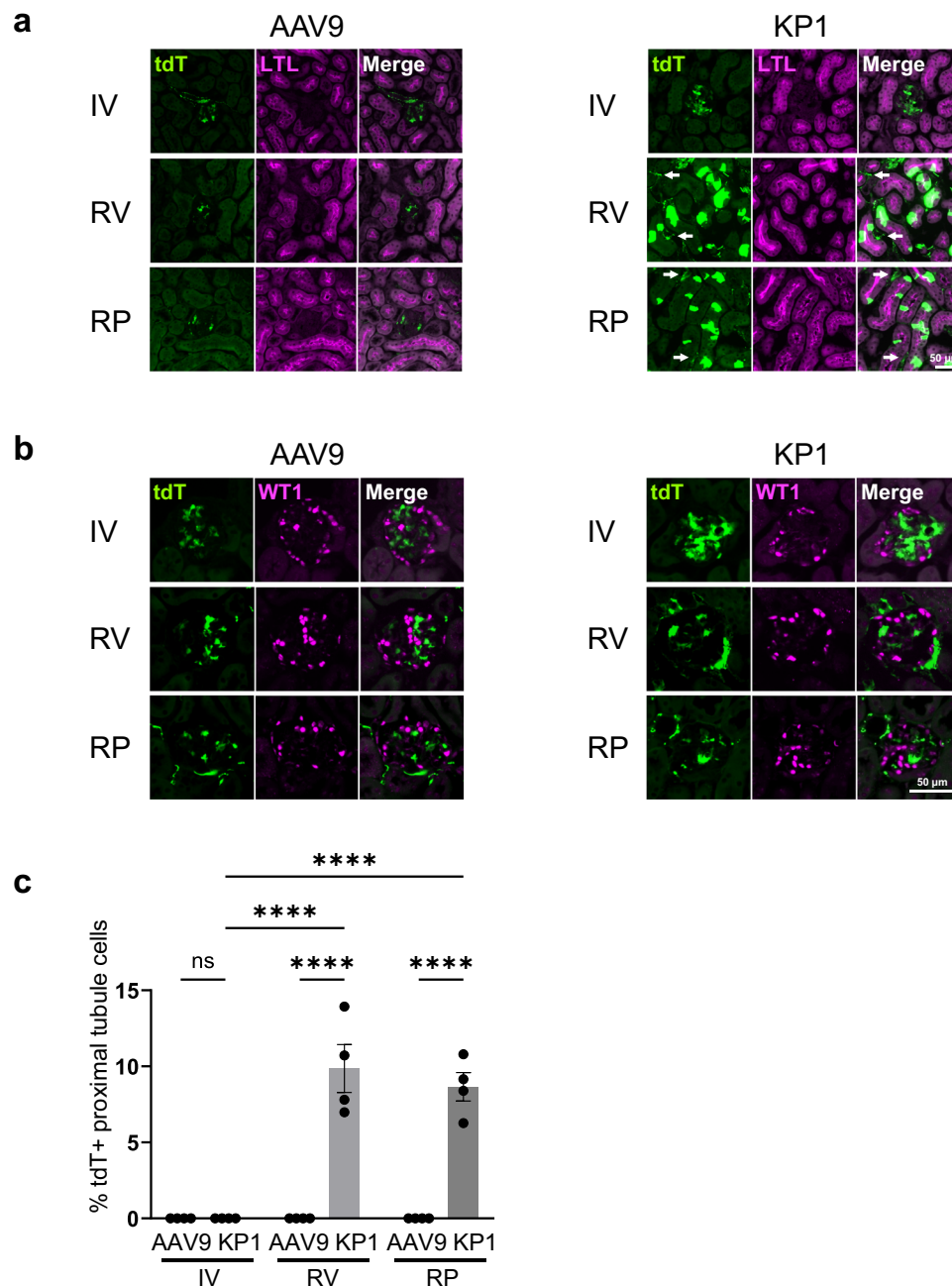
Fig. 3 | Enhanced transduction observed in proximal tubules by RV or RP injection of AAV-KP1, but not in podocytes. Eight-week-old C57BL/6 J male mice were injected with AAV9-CAG-tdTomato or AAV-KP1-CAG-tdTomato via IV, RV, or RP at a dose of 3.0×10^{11} vg/mouse ($n = 4$ per group). Kidneys were harvested 2 weeks post-injection for downstream analyses. **a, b** Representative fluorescence microscopic images of the AAV vector-treated mouse kidneys. In Panel (**a**), green and magenta colors represent native tdTomato fluorescence and LTL (a marker for proximal tubules), respectively. In Panel (**b**), green and magenta colors represent native tdTomato fluorescence and WT1 (a marker for podocytes), respectively. White arrows in Panel a (AAV-KP1/RV and AAV-KP1/RP groups) indicate transduction of interstitial cells. LTL, Lotus tetragonolobus lectin; WT1, Wilms tumor 1. Scale bars indicate 50 μm. **c** AAV9 and AAV-KP1 transduction efficiencies in the proximal tubules. The transduction efficiencies were assessed by manual counting of tdTomato-positive and negative proximal tubule cells labeled with anti-HNF4α antibody (a nuclear marker for proximal tubules). A two-way ANOVA followed by Tukey's post hoc test was used for statistical assessment of the data. ****, adjusted $p < 0.0001$; ns, not significant. Data are presented as mean ± standard error of the mean. Source data and exact p-values are provided in the Source Data file.

and the observed effective transduction of mesangial cells with AAV vectors. On the other hand, limited extravasation of microspheres from the peritubular capillary to the interstitial space was observed (indicated by arrows in Supplementary Fig. 5a). Next, we administered microspheres via RV and RP injections. Interestingly, both administration methods resulted in efficient interstitial accumulation of the microspheres, predominantly in the renal cortex (Supplementary Fig. 5c, d). It is important to note that interstitial accumulation was not observed by RP injection in the absence of the blockade of renal blood flow (Supplementary Fig. 5e). These observations suggest that the peritubular capillary wall poses a significant barrier for AAV vectors to transduce tubular epithelial cells following IV injection, while RV and RP injections allow AAV to pass through or bypass this barrier, leading to efficient transduction of the proximal tubules from the basolateral side. The lack of transduction enhancement by RP injection without local blockade of the blood flow (Supplementary Fig. 4c) also supports the importance of interstitial accumulation of AAV for proximal tubule transduction in mice.
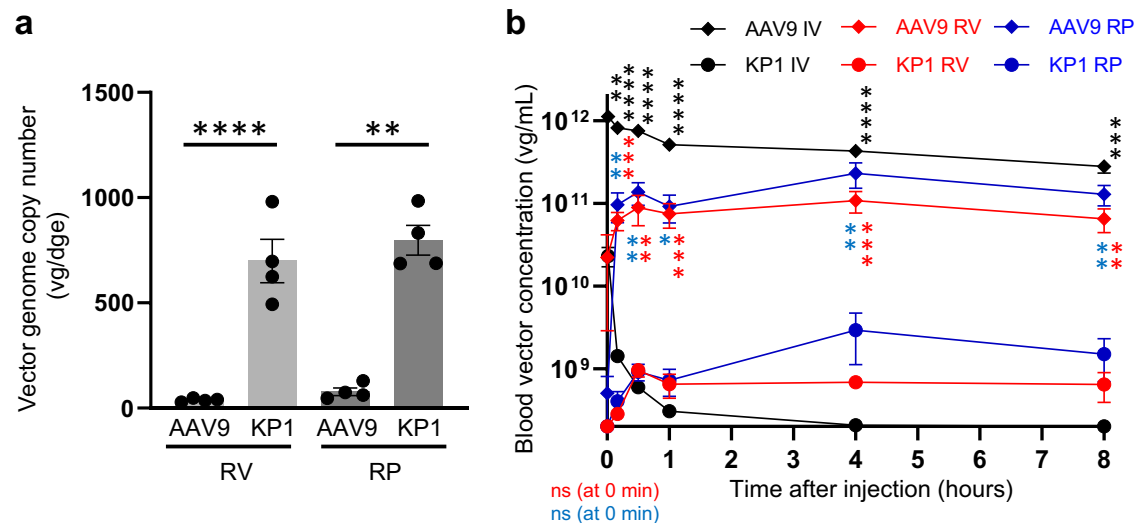
Fig. 4 | **AAV vector pharmacokinetics following RV or RP injection.** Eight-week-old C57BL/6 J male mice were injected with AAV9-CAG-tdTomato or AAV-KP1-CAG-tdTomato via IV, RV, or RP at a dose of 1.0×10^{13} vg/kg. $N = 4$ per group. **a** AAV vector genome copy numbers in the AAV vector-administered kidneys were determined by qPCR 10 min after RV or RP injection. Vector genome copy numbers are expressed as single-stranded (ss) vector genome copy numbers per diploid genomic equivalent (vg/dge). **b** Blood vector concentration-time curves following IV, RV, or RP injection. A two-tailed Welch's t test with Bonferroni correction was used. In Panel (**b**), the p-value indicates the statistical comparison between AAV9 and AAV-KP1 at each time point in each vector administration group. Please note that the first time points are 1 min for IV and 0 min for RV and RP injections. ****, adjusted $p < 0.0001$; ***, adjusted $p < 0.001$; **, adjusted $p < 0.01$; *, adjusted $p < 0.05$; ns, not significant. Data are presented as mean ± standard error of the mean. Source data and exact p-values are provided in the Source Data file.

Pharmacokinetics as a key determinant of off-target transduction

We hypothesized that the difference in pharmacokinetics following local injection leads to the contrasting renal and hepatic transduction between AAV9 and AAV-KP1 (Fig. 2). Quantification of vector genomes 10 min after local injection showed >10 times more vector genomes in the AAV-KP1-injected kidney than the AAV9-injected kidney following RV and RP injections (Fig. 4a). It is important to note that transduction with AAV vector does not occur within 10 min following vector exposure in vivo[22]. Thus, it is unlikely that the higher concentration of AAV-KP1 vector genomes in the injected kidney is the consequence of higher transduction. In addition, blood concentrations of AAV-KP1 were more than 50-fold lower than those of AAV9 throughout the study at all time points following the completion of vector administration (10 min, 30 min, 1 h, 4 h, and 8 h after RV and RP injections, Fig. 4b). These findings indicate that injected AAV-KP1 vector particles stay in the kidney more efficiently than AAV9 vector particles with limited spillover to systemic circulation. Please note that there is a peak at 4 h following RV and RP injections in the blood vector concentration curves (Fig. 4b). This pharmacokinetic profile mirrors that of subcutaneous injection, where AAV accumulates in the interstitial space of subcutaneous fat tissue and is gradually absorbed into the systemic circulation (absorption phase)[22], providing another evidence of interstitial accumulation following RV and RP injections.

Urinary excretion of AAV9 is increased in CKD

To successfully apply AAV vector approaches for the treatment of CKD, it is crucial to understand AAV vector transduction and pharmacokinetic profiles in CKD. To this end, we employed the Col4a5 mutant mouse model harboring a G5X nonsense mutation in the α5 chain of type IV collagen (B6.Cg-Col4a5[tm1Yseg]/J)[28], which serves as a mouse model of X-linked Alport syndrome. Hemizygous male mice of this strain manifest progressive renal failure due to Alport syndrome, which is the second most common genetic cause of CKD in adults[3]. To characterize in vivo AAV vector biology in this CKD mouse model, we injected 25 to 30-week-old B6.Cg-Col4a5[tm1Yseg]/J hemizygous male mice and age-matched wild-type mice from the colony with AAV9-CAG-

tdTomato or AAV-KP1-CAG-tdTomato vector via IV at a dose of 1.0×10^{13} vg/kg (~ 3.0×10^{11} vg/mouse, $n = 3$ to 5 per group, Fig. 5a). As reported previously[28], our hemizygous mutant male mice manifested significant albuminuria. Urinary albumin excretion of the mutant mice and the wild-type controls at the time of injection was 1.80 ± 0.14 g/gCre and 0.05 ± 0.01 g/gCre, respectively (two-tailed Welch's t test, $p = 3.4 \times 10^{-7}$, Fig. 5b), suggesting increased permeability of the glomerular filtration barrier in CKD kidney. To investigate whether the altered glomerular filtration barrier affects the pharmacokinetics of AAV vectors, we quantified urinary excretion of AAV over 5 h following IV injection of the AAV9 or AAV-KP1 vector. In the wild-type control mice, only about 0.001% of injected AAV9 and AAV-KP1 vector particles were excreted into the urine during the 5-h period (4.7×10^{5} to 1.5×10^{6} vg of a total of 3.0×10^{11} vg injected into each animal, Fig. 5c). In contrast, more than 1% of injected AAV9 vector particles (3.8×10^{9} to 9.5×10^{9} vg of a total of 3.0×10^{11} vg injected into each animal) were excreted in CKD mice, showing a 10^{4} times increase compared to the wild-type control mice (two-way ANOVA followed by Tukey's post hoc test, adjusted $p = 2.7 \times 10^{-5}$, Fig. 5c). Interestingly, unlike AAV9, the urinary excretion of AAV-KP1 in the CKD mouse model was only modestly increased with no statistical significance (two-way ANOVA followed by Tukey's post hoc test, adjusted $p = 0.10$, Fig. 5c). In line with this, AAV9 and AAV-KP1 showed distinct blood concentration following IV administration. In contrast to the delayed blood clearance of AAV9[22], AAV-KP1 was rapidly cleared from the bloodstream following IV administration, resulting in 48 times less blood concentration at 1 min and 572 to 2152 times less blood concentrations at the time points between 30 min and 8 h post-injection in the wild-type mice (Fig. 4b). We also observed 2034 times less blood concentration of AAV-KP1 compared to AAV9 in CKD mice at 8 h following IV administration (Supplementary Fig. 6), suggesting that contrasting pharmacokinetics of AAV9 and AAV-KP1 is maintained in CKD. Although the degree of glomerular filtration of substances is not solely determined by their blood concentrations, blood and urine concentrations of substances are positively correlated in many instances[29]. Therefore, it is reasonable to interpret that the contrasting urinary excretion profiles of AAV9 and AAV-KP1 are primarily attributed to the difference in their blood concentrations.
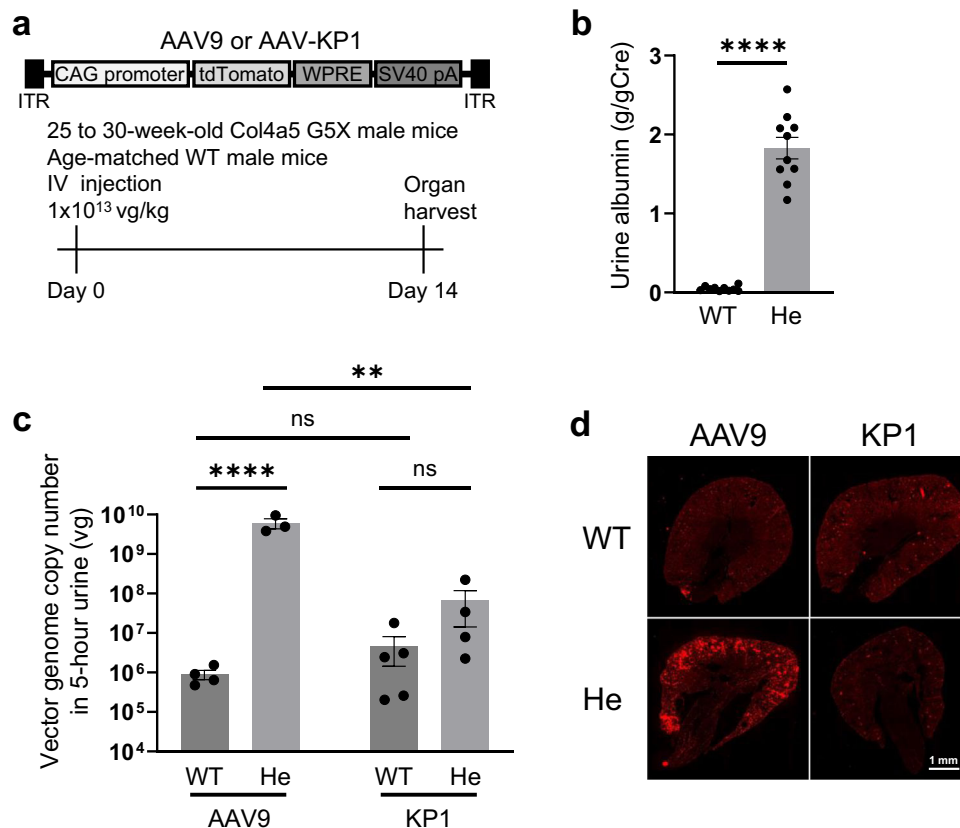
Fig. 5 | Enhanced AAV-vector mediated renal transduction and urinary AAV excretion in CKD following IV injection of AAV9. a The experimental design. **b** Albumin levels in the urine samples collected from the 25 to 30-week-old Col4a5 G5X hemizygous male mice (He) and age-matched wild-type control male mice (WT), at the time of injection ($n = 10$ each). The data was normalized by urine creatinine concentration and expressed as g/gCre. A two-tailed Welch's *t* test was used for statistical assessment. **c** Urinary excretion of AAV-CAG-tdTomato vectors over 5 h following IV injection. AAV vector genome copy numbers in urine samples were determined by qPCR in the following 4 groups: AAV9 in WT ($n = 4$), AAV9 in He ($n = 3$), AAV-KP1 in WT ($n = 5$) and AAV-KP1 in He ($n = 4$). A two-way ANOVA followed by Tukey's post hoc test was used for statistical assessment of the data. ****, $p < 0.0001$ or adjusted $p < 0.0001$; **, adjusted $p < 0.01$; ns, not significant. Data are presented as mean ± standard error of the mean. **d** Representative fluorescence microscopic images of the kidneys in the AAV-vector treated mice. Red, native tdTomato fluorescence. The scale bar indicates 1 mm. Source data and exact *p*-values are provided in the Source Data file.

Enhanced renal transduction by AAV9 IV injection in CKD

We next analyzed the renal transduction efficiency and cell type tropism of AAV9 and AAV-KP1 administered via IV in the CKD mouse model. Global renal transduction of the AAV9 vector was enhanced in the CKD kidney, which was not observed in the CKD mice injected with the AAV-KP1 vector (Fig. 5d). The enhanced transduction of AAV9 in the CKD kidney was mainly observed in the cortex. Co-staining of proximal tubules revealed that AAV9 transduced 9.3% of proximal tubules of the CKD kidney, while no proximal tubule transduction was observed in the wild-type control kidney (Fig. 6a, c). On the other hand, proximal tubule transduction was not observed in the CKD mice injected with the AAV-KP1 vector (Fig. 6b, c). Importantly, co-staining of podocyte nuclei revealed that AAV9 and AAV-KP1 transduced 35% and 15% of podocytes in the CKD kidney (Fig. 6b, d). The higher podocyte transduction with AAV9 than AAV-KP1 (two-way ANOVA followed by Tukey's post hoc test, adjusted $p = 0.011$) is consistent with the higher urinary excretion of AAV9 than AAV-KP1 in the CKD mice (Fig. 5c). We also investigated cardiac transduction with AAV9 and AAV-KP1 in CKD mice. We hypothesized that the cardiac transduction with AAV vectors could be affected in the CKD mice as CKD has a systemic effect, especially on cardiovascular organs[30], and cardiac remodeling such as hypertrophy, fibrosis, capillary rarefaction is a common feature of CKD, including Alport syndrome[31–33]. The results showed significantly enhanced cardiac transduction with AAV9 in the CKD mice compared to the wild-type mouse controls (two-way ANOVA followed by Tukey's post hoc test, adjusted $p = 0.018$, Supplementary

Fig. 7). On the other hand, there was no difference in cardiac transduction between the CKD mice and the wild-type controls injected with AAV-KP1 (two-way ANOVA followed by Tukey's post hoc test, adjusted $p = 0.99$, Supplementary Fig. 7) presumably due to the low cardiac tropism of AAV-KP1 compared to AAV9 (two-way ANOVA followed by Tukey's post hoc test, adjusted $p = 0.046$, Supplementary Fig. 7). We also administered AAV9 and AAV-KP1 via RP in CKD mice. No proximal tubule or podocyte transduction was observed when AAV9 or AAV-KP1 was administered via the RP route in CKD mice (Supplementary Fig. 8). These observations underscore the importance of the host condition as a key determinant of AAV vector transduction, with varying effects among different AAV capsids (see Supplementary Discussion 2).

Effective AAV9 and AAV-KP1 transduction in NHP kidneys via RP

To translate our findings of RP injection in the primate context, we developed a real-time image-guided retrograde transureteral RP injection procedure in rhesus macaques, as outlined in the Materials and Methods section. The procedure was performed on 7 female rhesus macaques, summarized in Supplementary Table 2. In the first set of experiments, we administered AAV-KP1 and AAV9 via RP in respective neutralizing antibody (NAb)-negative or marginally positive NHPs: two (NHP2 and NHP3) received AAV-KP1-CAG-tdTomato and one (NHP4) received AAV9-CAG-tdTomato. One animal (NHP1) received the vehicle only. Blood samples were collected at multiple time points on the day of injection for a pharmacokinetic analysis, and
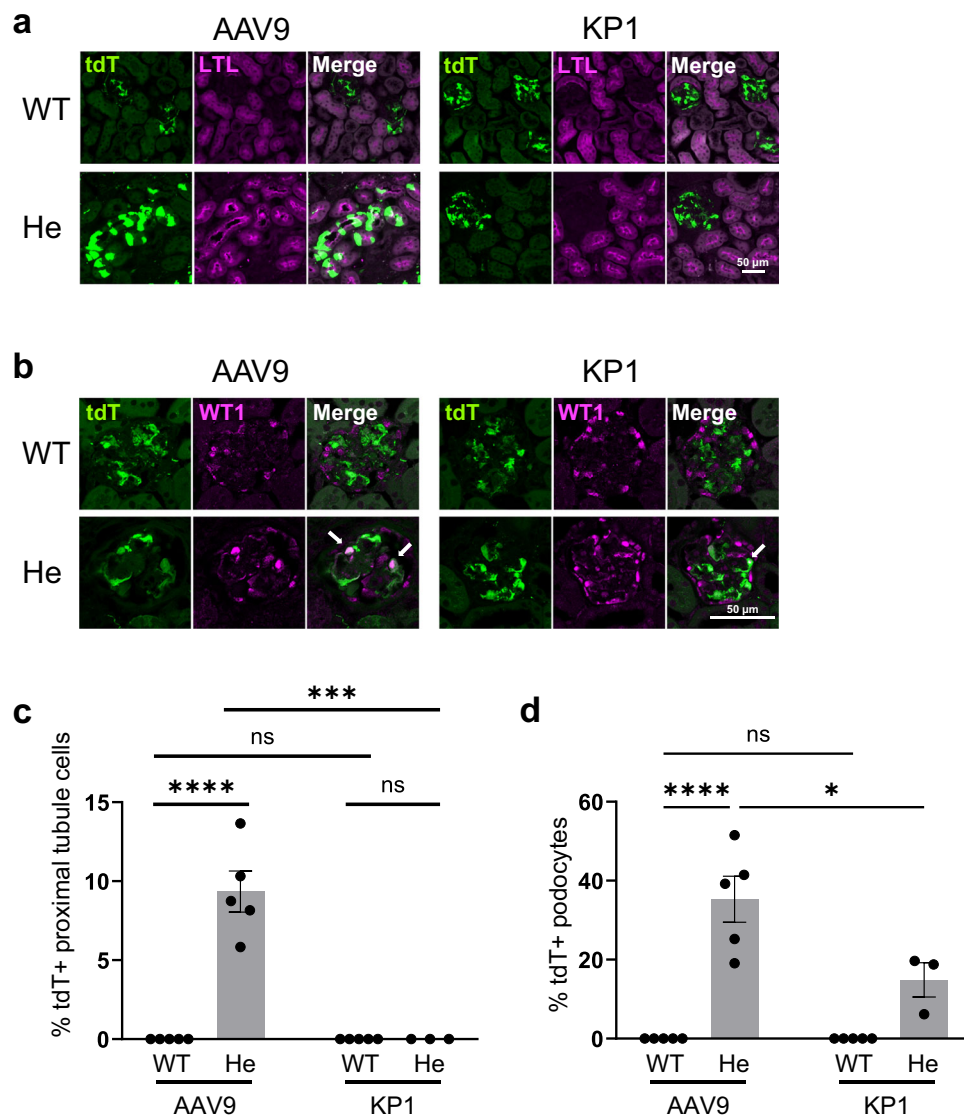
Fig. 6 | Enhanced AAV9-mediated transduction of proximal tubules and podocytes in CKD kidney following IV injection. Twenty-five to 30-week-old Col4a5 G5X hemizygous male mice (He) and age-matched wild-type control male mice (WT) were injected with AAV9-CAG-tdTomato and AAV-KP1-CAG-tdTomato via IV at a dose of 1.0×10^{13} vg/kg. Kidneys were harvested 2 weeks post-injection for downstream analyses. AAV9 in WT ($n = 5$), AAV9 in He ($n = 5$), AAV-KP1 in WT ($n = 5$) and AAV-KP1 in He ($n = 3$). **a, b** Representative fluorescence microscopic images of the kidneys in the AAV vector-treated mice. In Panel (**a**), green and magenta colors represent native tdTomato fluorescence and LTL (a marker for proximal tubules), respectively. In Panel (**b**), green and magenta colors represent native tdTomato fluorescence and WT1 (a marker for podocytes), respectively. White arrows indicate AAV vector-transduced podocytes. Scale bars indicate 50 μm. **c** AAV9 and AAV-KP1 transduction efficiencies in the proximal tubules. The transduction efficiencies were assessed by manual counting of tdTomato-positive and negative proximal tubule cells labeled with anti-HNF4α antibody (a nuclear marker for proximal tubules). **d** AAV9 and AAV-KP1 transduction efficiencies in podocytes. The transduction efficiencies were assessed by manual counting of tdTomato-positive and negative podocytes labeled with anti-WT1 antibodies. A two-way ANOVA followed by Tukey's post hoc test was used for statistical assessment of the data. ****, adjusted $p < 0.0001$; ***, adjusted $p < 0.001$; *, adjusted $p < 0.05$; ns, not significant. Data are presented as mean ± standard error of the mean. LTL, Lotus tetragonolobus lectin; WT1, Wilms tumor 1. Source data and exact p-values are provided in the Source Data file.
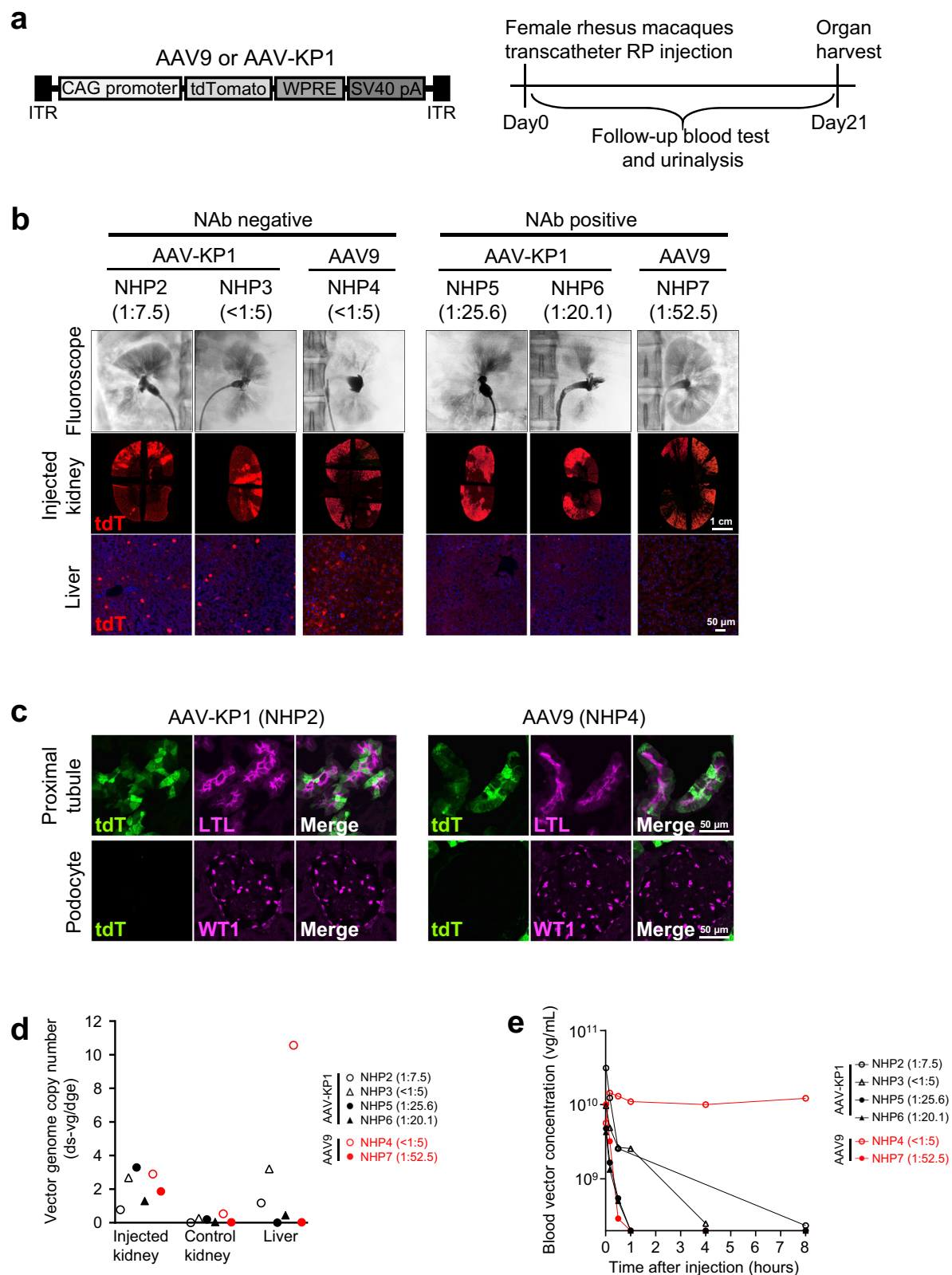
tissues were harvested for the assessment of AAV vector transduction and biodistribution 3 weeks post-injection (Fig. 7a). In contrast to the mouse study, both AAV-KP1 and AAV9 showed efficient cortical transduction in the area that corresponds to the injection path that was visualized by fluoroscopy performed shortly before AAV vector injection (Fig. 7b). The cortical transduction observed in AAV-KP1-injected and AAV9-injected kidneys was primarily attributable to exclusive transduction in proximal tubules, with no glomerular cell involvement including podocytes (Fig. 7c and Supplementary Fig. 9). As observed in the mouse study, blood concentration of AAV9 (NHP4) was higher than that of AAV-KP1 (NHP2 and NHP3) following RP injection (Fig. 7e), and accordingly, more off-target liver transduction was observed in

AAV9-treated NHP compared to AAV-KP1-treated NHPs (Fig. 7b, d). However, unlike in mice, no absorption phase was observed in NHPs, with blood vector concentrations reaching a peak immediately after injection (Fig. 7e).

RP injection overcomes pre-existing immunity in NHPs

Even low titers of pre-existing anti-AAV NAbs abolish in vivo transduction with AAV vectors in mice and NHPs when administered systemically[34,35]. On the other hand, local injection of an AAV vector into immune-privileged organs such as the eyes and central nervous system (CNS) can allow successful transduction in target cells in the presence of NAbs in the blood circulation. Immunoglobulin

a AAV9 or AAV-KP1: ITR — CAG promoter — tdTomato — WPRE — SV40 pA — ITR

Female rhesus macaques transcatheter RP injection → Organ harvest; Day0 → Day21; Follow-up blood test and urinalysis

b NAb negative / NAb positive

AAV-KP1: NHP2 (1:7.5), NHP3 (<1:5); AAV9: NHP4 (<1:5); AAV-KP1: NHP5 (1:25.6), NHP6 (1:20.1); AAV9: NHP7 (1:52.5)

Rows: Fluoroscope; Injected kidney (tdT, scale 1 cm); Liver (tdT, scale 50 μm)

c AAV-KP1 (NHP2) / AAV9 (NHP4)

Proximal tubule (tdT, LTL, Merge, 50 μm); Podocyte (tdT, WT1, Merge, 50 μm)

d Vector genome copy number (ds-vg/dge): Injected kidney, Control kidney, Liver

AAV-KP1: NHP2 (1:7.5), NHP3 (<1:5), NHP5 (1:25.6), NHP6 (1:20.1); AAV9: NHP4 (<1:5), NHP7 (1:52.5)

e Blood vector concentration (vg/mL) vs Time after injection (hours)

AAV-KP1: NHP2 (1:7.5), NHP3 (<1:5), NHP5 (1:25.6), NHP6 (1:20.1); AAV9: NHP4 (<1:5), NHP7 (1:52.5)

concentration in cerebrospinal fluid is one thousand times less than that in plasma[36]. Accordingly, it was shown that the presence of anti-AAV NAbs of up to 1:128 in the blood does not block transduction in the CNS when administered intrathecally[37]. As immunoglobulin concentration in the urine is also more than one thousand times less than that in the plasma[38], we hypothesized that RP injection can evade pre-existing humoral immunity against AAV. To address this, we

administered AAV-KP1-CAG-tdTomato or AAV9-CAG-tdTomato via RP injection into three female rhesus macaques harboring NAbs to the corresponding AAV capsids at a titer of 1:25.6 (NHP5, AAV-KP1), 1:20.1 (NHP6, AAV-KP1) and 1:52.5 (NHP7, AAV9), and renal and hepatic transduction was assessed 3 weeks post-injection. As shown in Fig. 7b, robust transduction was observed in the cortex of the kidney of all three NHPs despite the presence of pre-existing NAbs. Transduction

Fig. 7 | Robust proximal tubule transduction following transcatheter RP injection of AAV-KP1 and AAV9 in NHPs regardless of anti-AAV NAbs. a The experimental design. **b** Fluoroscopic images, immunofluorescence microscopic images for native tdTomato (red) in the longitudinal sections of the injected kidneys and in the off-target livers from the 6 animals injected with AAV-KP1-CAG-tdTomato (*n* = 4) or AAV9-CAG-tdTomato (*n* = 2) via RP. For fluoroscopic images, a contrast agent was injected into the renal pelvis through the catheter to visualize the injection path. Note that the same orientations were used for the fluoroscopic images and the immunofluorescence images of the longitudinal sections. For the livers, one section from each of the right and left lobes was examined, and a representative image was shown. Blue, DAPI. **c** Representative high-magnification images of the kidneys from 2 animals: one injected with AAV-KP1-CAG-tdTomato (NHP2) and another with AAV9-CAG-tdTomato (NHP4). The whole longitudinal section was examined, and a representative image from the transduced area was shown. Colors represent native tdTomato fluorescence (green) with LTL (magenta, a marker for proximal tubules) or WT1 (magenta, a marker for podocytes). LTL, Lotus tetragonolobus lectin; WT1, Wilms tumor 1. The transduction data for the other 4 NHPs are provided in Supplementary Fig. 9. Scale bar in the longitudinal sections of the injected kidneys indicates 1 cm. Other scale bars indicate 50 μm. **d** AAV vector genome copy numbers in the AAV vector-injected kidneys, control (contralateral uninjected) kidneys, and livers determined by qPCR. Vector genome copy numbers are expressed as ds-vg/dge. **e** Blood vector concentration-time curves following RP injection. Please note that blood vector concentration was not assessed at 1 h, 4 h (NHP2), and 8 h (NHP3) due to sample unavailability. Numbers in parentheses indicate NAb titers. Source data are provided in the Source Data file.

pattern was also segmental corresponding to the injection path (Fig. 7b), showing efficient proximal tubule transduction and no glomerular transduction (Supplementary Fig. 9). Vector genome copy numbers in the kidney also showed comparable levels regardless of NAbs titers (Fig. 7d). Importantly, off-target liver transduction was suppressed in both AAV-KP1 (NHP5 and NHP6) and AAV9 (NHP7) injected NHPs in the presence of NAbs (Fig. 7b, d), in which AAV was cleared from the blood circulation more rapidly than those in NHPs without NAbs (Fig. 7e). This accelerated clearance is presumed to result from the swift removal of neutralized viral particles by the host immune mechanisms. We also conducted a study investigating whether AAV-KP1 injection via RP can overcome pre-existing anti-AAV-KP1 humoral immunity in mice, showing no successful kidney transduction in the presence of NAbs (Supplementary Table 3).

Safety considerations on RP injection

This RP procedure was performed safely on all seven NHPs with no major clinical complications or procedural failure. There was a modest elevation of liver enzymes one day post-injection in all animals, but it was resolved within a week (Supplementary Table 4). This is most likely procedure-related rather than AAV vector-related toxicity, as the NHP injected with the vehicle only (NHP1) also manifested an elevation of liver enzymes. In the cortex of the injected kidneys, infiltration of mononuclear cells and tubulitis with no glomerular involvement were sometimes observed in the transduced area (NHP2, NHP4, NHP6, and NHP7, Supplementary Fig. 10, see Supplementary Discussion 3). The contralateral kidney or the kidney injected with the vehicle only (NHP1) did not show this pathological change.

Discussion

In this study, we have identified a small subset of AAV capsids, including AAV-KP1 that exhibit significantly enhanced gene transfer to the kidney by local vector administration in mice and revealed key differences in renal transduction profiles between healthy and CKD kidneys as well as between mice and NHPs. According to the previous studies assessing renal transduction of common AAV serotypes by IV[6,7], RV[10], and RP[12–14,39,40] injections, AAV9 has been generally regarded as one of the most efficient capsids across various administration routes. However, our study has demonstrated that optimal AAV capsids are not necessarily the same between systemic and local injections. AAV-KP[17] and AAV-DJ[19] were generated by capsid shuffling and in vitro screening in pancreatic islet and hepatoma cells, respectively. AAV2G9 was generated by engraftment of the galactose binding motif in the AAV9 capsid into the AAV2 capsid[20]. AAV2.7m8 was generated by an in vivo screen of AAV capsid mutants in photoreceptors of the mouse retina[21]. Therefore, their high performance in renal gene transfer by local administration was unexpected and unpredictable. Thus, this study underscores the importance of comprehensive AAV capsid characterization in renal gene delivery across diverse contexts using robust approaches such as AAV Barcode-Seq.

One of the key findings in our study using mice is that AAV-KP1 efficiently transduces the proximal tubules by local vector administration. The proximal tubules, which account for about half of the tubular epithelial cells[41], are a crucial target for both basic research[42] and gene therapy[5]. Importantly, RV and RP injections are not parenchymal, thus avoiding restricted vector spread and tissue damage. These injections allow AAV vectors to infiltrate the entire kidney, achieving widespread proximal tubule transduction. Unlike previous studies[10,13,14], our work shows that extended renal blood flow blockade is not necessary for efficient renal transduction with AAV-KP1. In addition, AAV-KP1 exhibits a unique phenotype that minimizes off-target effects. In contrast to AAV9, which shows significant spillover to off-target organs, including the liver following local administration[43,44], AAV-KP1 efficiently accumulates at the injection site and minimizes systemic vector dissemination. Given the growing concerns about AAV-related toxicity in humans, including hepatotoxicity, genotoxicity, thrombotic microangiopathy, and DRG toxicity[1,15,45], local administration of AAV-KP1 and other capsids showing similar phenotypes offers a promising approach to mediate effective renal gene delivery while mitigating these risks.

Another key finding is that IV injection of AAV9 effectively transduces podocytes and proximal tubules at levels of 35% and 9.3%, respectively, in the CKD mouse model. To date, two studies have used AAV9 vectors to deliver therapeutic genes to the kidney in mouse models of autosomal recessive Alport syndrome[46] and nephrotic syndrome[8]. However, these studies did not assess differences in transduction between healthy and diseased kidneys; therefore, the potentially multifaceted effects of CKD on AAV transduction remained unknown. Given that podocytes represent the common target cell type for monogenic kidney diseases[5,47], and AAV9 has been used as a clinical IV product already approved by regulatory agencies, the demonstration of the ability of a modest dose of AAV9 to transduce approximately one-third of podocytes in CKD holds immense clinical implications if this is also the case in humans. Although detailed mechanisms for enhanced podocyte transduction in CKD will be the focus of future studies, our data suggest that the increased permeability of the glomerular filtration barrier plays a crucial role. The difference in proximal tubule transductions in CKD between AAV9 and AAV-KP1 is presumably explained by the difference in their pharmacokinetic profiles. A previous study has shown that the peritubular capillary undergoes functional and structural changes in CKD, with the increased permeability of the peritubular capillary being a common feature of CKD, including Alport syndrome[48]. Thus, in the CKD kidney, AAV9's delayed blood clearance should provide a greater opportunity for a larger quantity of vector particles to pass through the compromised peritubular capillary wall compared to AAV-KP1. This disparity in the pharmacokinetics presumably allows AAV9 to transduce more proximal tubules than AAV-KP1 from the interstitial basolateral side (Fig. 8). On the other hand, transduction from the apical side by the increased urinary concentration of AAV9 is unlikely as RP injection of AAV9 failed to transduce proximal tubules in CKD.
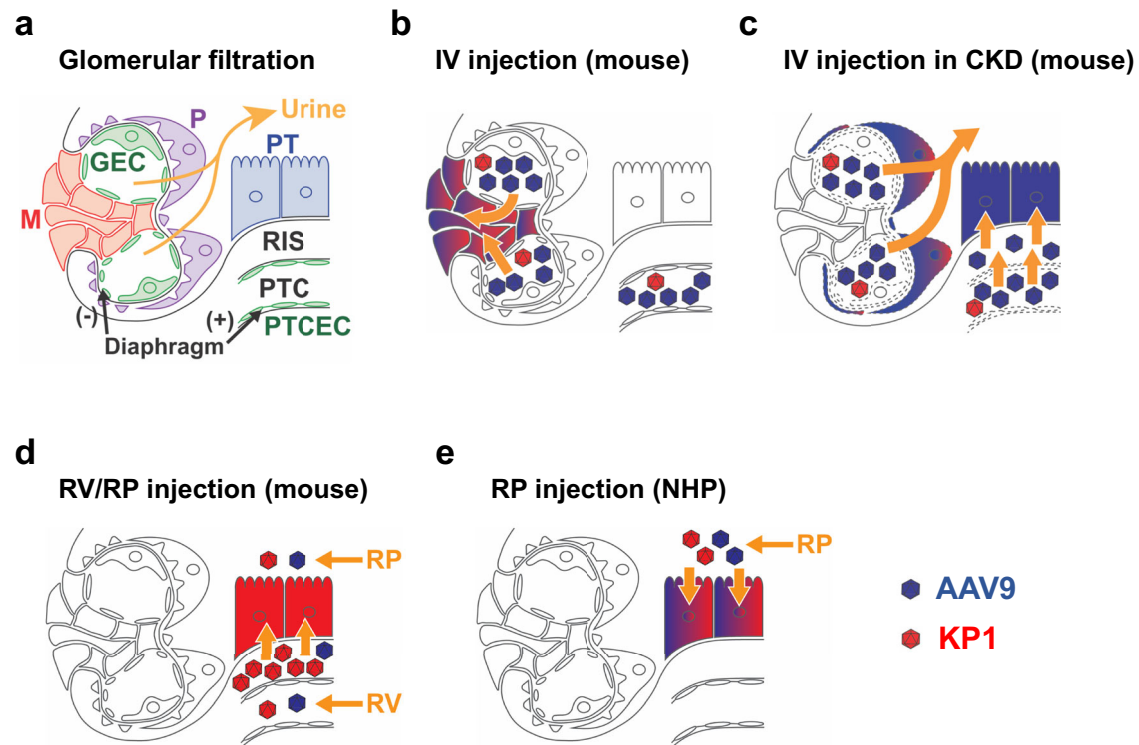
Fig. 8 | A mechanistic model of AAV9 and AAV-KP1-mediated renal transduction. a Glomerular filtration occurs across the glomerular endothelial cells (GEC), the glomerular basement membrane and podocytes (P). The filtration flow is indicated with yellow arrows. The renal interstitial space (RIS) is the space between the proximal tubules (PT) and the peritubular capillaries (PTC). M, mesangial cell; PTCEC, peritubular capillary endothelial cell. **b–e** Cells transduced with AAV9 and AAV-KP1 are highlighted in the corresponding colors. **b** Upon IV injection in healthy mice, glomerular filtration of AAV is prevented in the kidney. AAV is preferentially distributed into the M area through the fenestrae of GEC that lacks both a diaphragm and a basement membrane. **c** Upon IV injection in CKD mice, the impaired glomerular filtration barrier and PTC barrier (indicated by dashed lines) enhance AAV excretion into the urine (Fig. 5c) and promote AAV extravasation into RIS. This enables enhanced transduction of P and PT following IV injection. Both AAV9 and AAV-KP1 transduce P, with AAV9 exhibiting higher transduction efficiency (Fig. 6b, d). On the other hand, only AAV9, not AAV-KP1, transduces PT (Fig. 6a, c). This is because AAV9 crosses the barriers more efficiently than AAV-KP1 due to its delayed blood clearance following IV injection (Fig. 4b). **d** Upon RV and RP injections in healthy mice, AAV can reach RIS (Supplementary Fig. 5). However, only AAV-KP1, not AAV9, can accumulate in RIS due to its unique attribute (Fig. 4a), and achieves PT transduction (Figs. 3a and 3c). The strong accumulation of AAV-KP1 also reduces vector spillover into the blood circulation, minimizing vector dissemination to off-target organs (Figs. 2b, d, and 4b). Note that PT transduction does not occur by RP injection of AAV9 or AAV-KP1 in CKD mice. Transduction of M occurs in Panels (**c**, **d**), but this is not depicted in this schematic. **e** Upon catheter-based RP injection in NHPs, both AAV9 and AAV-KP1 transduce PT, most likely from the apical side.

Our NHP study demonstrated that the local administration of AAV vectors via RP holds promise for clinical application. Importantly, the procedure can be performed using standard clinical equipment; therefore, it is readily applicable in a clinical setting. With this approach, efficient transduction in cortical proximal tubules was consistently achieved with both AAV9 and AAV-KP1, even in the presence of anti-AAV NAbs. Pre-existing NAbs may even be beneficial in terms of minimizing off-target organ transduction as AAV vectors are rapidly cleared from the blood circulation by NAbs before reaching off-target organs such as the liver. This is consistent with the previous study demonstrating that even low levels of NAbs (at a titer of 1:4) can prevent the transduction of AAV vector administered intravenously[34,35]. For those without NAbs, it may be an option to combine passive immunization using IVIG with RP injection to reduce the off-target effect as used with intrathecal AAV administration[49]. Pre-existing immunity to AAV vector remains a major limitation of AAV-mediated gene therapy, and individuals with NAbs that account for up to 40% of the adult population[50] are normally excluded from the therapy-eligible groups. Several strategies have been developed that include the use of less antigenic AAV capsids generated by capsid engineering[19,51], pharmacological intervention with immunosuppressants[52] or removal of immunoglobulins from the bloodstream by plasmapheresis and immunoadsorption[53] or intravenous administration of an IgG-cleaving enzyme[54,55]. However, their clinical efficacies have yet to be determined. RP administration does not require such interventions and, therefore, could potentially expand the applicability of AAV-mediated renal gene therapy, including repeated dosing.

Our study offers a unique opportunity to compare AAV transduction and pharmacokinetics profiles for renal gene transfer between mice and NHPs. In the context of RP injection, we have identified the following five key differences between the two species. First, the blockade of the renal blood flow was essential for proximal tubule transduction in mice, while it was not required in NHP. Second, AAV9 administered via RP injection effectively transduced the proximal tubules of NHP kidneys, in stark contrast to mice, where no renal tubule transduction was observed. Third, no vector absorption phase was observed in NHPs, whereas mice exhibited an absorption phase with peak vector concentrations in the blood around 4 h post-injection. Fourth, the proximal tubule was homogeneously transduced in NHP kidneys rather than scattered transduction observed in mouse kidneys. Fifth, pre-existing anti-AAV humoral immunity can be overcome by RP injection in NHPs, but not in mice. Based on these observations, we propose that proximal tubule transduction via RP is primarily mediated by basolateral transduction with AAV accumulated in the interstitial space in mice, while direct vector entry from the urinary (apical) side is the main pathway for transduction in NHPs. This explains why blockade of the renal blood flow that facilitates interstitial accumulation of AAV vectors was not required in NHPs. This also

explains why RP-mediated renal tubule transduction with AAV9 and AAV-KP1 shows comparable efficacy in NHPs, despite their contrasting abilities to accumulate in the interstitial space. Moreover, the apical pathway is more direct than the accumulation-based pathway proposed in mice, leading to more homogeneous tubule transduction in NHPs. Furthermore, the apical pathway minimizes interactions between AAV and blood or interstitial fluid containing anti-AAV NAbs, thereby enabling escape from neutralization in NHPs.

Based on all the observations, we propose a mechanistic model for AAV vector-mediated renal transduction via IV, RV, and RP in mice and via RP in NHPs (Fig. 8). This model underscores the roles of kidney microanatomy, vector pharmacokinetics, and distinct AAV entry routes into renal tubules between mice and NHPs. The fenestrae of the glomerular endothelial cells lack a diaphragm[23], and there is no basement membrane between the glomerular capillary and the mesangium[24,25] (Fig. 8a). This unique architecture facilitates efficient mesangial transduction following IV injection (Fig. 8b). On the other hand, the pathway from the peritubular capillary to the tubular epithelial cells is composed, in series, of a fenestrated endothelium with a diaphragm, the capillary basement membrane, the interstitium and the tubular basement membrane[26,56]. This architecture makes tubular epithelial cell transduction by systemic delivery more challenging. In CKD, increased permeability of the compromised glomerular filtration barrier and peritubular capillaries allows AAV to reach podocytes via the glomerular filtrate and access renal tubules from their basolateral side through the interstitial space, respectively (Fig. 8c). In the RV and RP injections in mice, both AAV9 and AAV-KP1 are distributed to the interstitial space; however, only AAV-KP1 remains within the interstitial space efficiently and transduces the proximal tubules from the basolateral surface without undergoing rapid redistribution to the systemic circulation via venules or the lymphatic system (Fig. 8d). Our AAV Barcode-Seq data has shown similar transduction profiles across all the 47 different AAV capsids by RV and RP injections, suggesting the shared pathway between the two anatomically distinct administration routes. The shared pathway is likely the interstitial accumulation and the subsequent transduction of renal tubule cells from the basolateral side. To support this, RV and RP injections of AAV-KP1 also resulted in interstitial transduction in mice. Please note that our model does not address the specific mechanism by which AAV accumulates in the renal interstitium following RV and RP injections. We assume that the increased hydrostatic pressure in the peritubular capillaries and urinary lumens allows AAV to traverse across the endothelial and epithelial barriers that are transiently opened by the pressure and accumulate in the interstitial space. In NHP, AAV directly enters the tubular cells from their apical surface, leading to effective tubular transduction (Fig. 8e).

To make AAV fully effective for renal gene therapy, there are remaining hurdles to overcome. Among them, the packaging capacity of AAV vectors (up to ~5 kb) is the major limitation when targeting common genetic kidney diseases such as autosomal dominant polycystic kidney diseases (ADPKD) and Alport syndrome. Both diseases result from loss-of-function mutations in their causative genes, and transgenic animal models previously showed successful phenotype recovery by re-induction of gene expression[57,58], making these diseases candidates for gene therapy. However, the lengths of therapeutic genes for gene replacement therapy for ADPKD and Alport syndrome exceed the packaging capacity. Potential solutions include the use of multiple vectors with a protein trans-splicing system[59], gene miniaturization[60,61], and gene editing by CRISPR-Cas9[62]. Notably, the latter two methods have recently shown clinical success. The combination of these strategies and enhanced gene delivery shown in this study will broaden the target of AAV-mediated renal gene therapy. Although AAV transduces proximal tubules more effectively than distal nephrons, extending the transduction to the distal nephron is also important to treat ADPKD, whose cysts can originate from any part of the nephron.

In summary, the present study highlights the importance of AAV capsid selection depending on the route of administration and the host condition in the context of AAV vector-mediated renal gene delivery. Further research on context-dependent capsid engineering and characterization is imperative for the development of more effective and safer AAV vector-mediated gene delivery to the kidney.

Methods

AAV vectors and plasmids

AAV-CAG-VBC library, AAV9-CAG-tdTomato, AAV-KP1-CAG-tdTomato, and AAV-KP1-CAG-nlsGFP were produced in HEK293 cells (RRID: CVCL-6871, Agilent) by an adenovirus-free plasmid transfection method and purified by two rounds of cesium chloride density-gradient ultra-centrifugation followed by dialysis as described previously[63]. AAV9 and AAV-KP1 helper plasmids were provided by J. M. Wilson and M. A. Kay, respectively. pAAV-CAG-tdTomato and pAAV-CAG-nlsGFP were gifts from E. Boyden and V. Gradinaru (59462 and 104061, Addgene, Watertown, MA), respectively. For AAV barcode library production, we used pdsAAV-CAG-VBCx plasmids (where VBC is the viral barcode and x is an integer identification number indicating each different viral barcode contained in each plasmid). pdsAAV-CAG-VBCx plasmids are double-stranded (ds) AAV vector plasmids and same as pdsAAV-U6-VBCx described previously[63] except that the human U6 small nuclear RNA gene promoter has been replaced by the CAG promoter and a SV40 polyadenylation signal has been incorporated. For 47 AAV capsids in the library (Supplementary Table 1), we used a total of 114 barcodes. Two barcoded capsid clones were allocated to each capsid except for AAV9 and AAV2R585E, for which 15 and 9 barcoded clones were allocated, respectively. Each AAV capsid clone was produced in separate culture vessels. Subsequently, all the produced clones were mixed into a pool after titer adjustment and purified to create an AAV library stock as described elsewhere[16].

Mouse experiments

All the mouse experiments were performed according to the guidelines for animal care at Oregon Health & Science University (OHSU). Mice were kept with free access to food (5LOD, LabDiet, St. Louis, MO) and water in a controlled environment (12-h light-dark cycle with an average humidity range of 30–70% and temperatures of 20–23 °C). C57BL/6 J mice and B6.Cg-Col4a5^{tm1Yseg}/J mice were purchased from the Jackson Laboratory (Strain IDs are 664 and 6183, respectively). For the AAV Barcode-Seq analysis, 8-week-old C57BL/6 J male mice were injected with the AAV barcode library via the tail vein at a dose of 2.0×10^{13} vg/kg ($n = 3$), and via a renal vein ($n = 4$) and renal pelvis ($n = 3$) at a dose of 3.0×10^{11} vg/mouse. Six weeks post-injection, mice were euthanized, and kidneys were harvested. For the AAV9 and AAV-KP1 individual capsid validation study, 8-week-old C57BL/6 J male mice were injected with AAV9-CAG-tdTomato or AAV-KP1-CAG-tdTomato via the tail vein (*i.e.*, IV injection), renal vein (RV), and renal pelvis (RP) at a dose of 3.0×10^{11} vg/mouse ($n = 4$ per group). Two weeks post-injection, mice were euthanized, and kidneys and livers were harvested for vector genome quantification and histological assessment by immunofluorescence microscopy. For a pharmacokinetic study, 8-week-old C57BL/6 J male mice were injected with AAV9-CAG-tdTomato or AAV-KP1-CAG-tdTomato via IV, RV, or RP injection at a dose of 1.0×10^{13} vg/kg ($n = 4$ per group). Subsequently, whole blood samples were collected from the retro-orbital plexus at 6-time points (0 min for RV and RP when the 15-min dwelling was completed or 1 min for IV, followed by 10 min, 30 min, 1 h, 4 h, and 8 h) following vector injection, and vector genome copy numbers in the blood samples were determined as detailed in the AAV vector genome quantification section. To quantify vector genome copy numbers in the kidney after local vector injection, 8-week-old C57BL/6 J male mice were injected with AAV9-CAG-tdTomato or AAV-KP1-CAG-tdTomato via RV or RP injection at a dose of 1.0×10^{13} vg/kg ($n = 4$ per group). Subsequently, injected

kidneys were harvested 10 min after the completion of 15-min dwelling time following the RV and RP injections, and vector genome copy numbers in the kidney were determined as detailed in the AAV vector genome quantification section. To investigate the renal transduction in CKD, 25 to 30-week-old B6.Cg-Col4a5^{tm1Yseg}/J hemizygous male mice and age-matched wild-type controls from the colony were randomly allocated to two groups and intravenously injected with AAV9-CAG-tdTomato or AAV-KP1-CAG-tdTomato at a dose of 1.0×10^{13} vg/kg ($n = 3$–5 per group). After injection, mice were put in the metabolic cage (MMC100, Hatteras Instruments, Grantsboro, NC) for 5 h to collect the urine samples. Two weeks post-injection, mice were euthanized, and the kidneys and hearts were harvested for downstream analysis. For active immunization with AAV-KP1, 20-week-old C57BL/6 J male mice were injected via IV with AAV-KP1-CAG-nlsGFP at a dose of 2.3×10^{11} vg/mouse and incubated for 3 weeks for anti-AAV-KP1 antibody production. For passive immunization with AAV-KP1, six 11-week-old C57BL/6 J male mice were injected via IV with AAV-KP1-CAG-tdTomato at a dose of 1.0×10^{11} vg/mouse. Four weeks post-injection, sera were collected from these mice, pooled, and kept frozen until use. Passive immunization of mice was then established by infusing 100 μL of the pooled sera immediately before the experimental treatment. As a control, one mouse received 100 μL of naive mouse sera instead of the anti-sera and was subjected to the same experimental treatment. To address sex as a biological variable, we injected the AAV-KP1-CAG-tdTomato vector into C57BL/6 J female mice via RV ($n = 2$) and RP ($n = 3$).

Mouse surgical procedures

For RV injection, modified from the previous protocol[10], mice were anesthetized by isoflurane inhalation and placed on a heated surgical pad (8002062012, Stryker Medical, Portage, MI) to maintain a constant body temperature. A medial abdominal incision was made, and intestines were removed from the abdominal cavity to expose the left renal vasculature and the kidney. Removed intestines were kept moist throughout the surgery. A non-traumatic micro-serrefine clamp was placed on the renal artery and vein, and 50 μL of AAV vector solution was injected using a 31-gauge needle (328468, BD Medical, Franklin Lakes, NJ) by hand as quickly as possible. Following the 15-minute ischemic time, the clamp was removed to observe the restoration of the blood flow (verified by color change), and the incision was closed. For RP injection, modified from the previous protocol[64], a flank incision was made to expose the left kidney to place a non-traumatic micro-serrefine clamp on the renal pedicle and the ureter under general anesthesia. Fifty μL of AAV solution was injected into the pelvic cavity over 1 min using a syringe pump (70-4507, Harvard Apparatus, Holliston, MA) to prevent parenchymal damage and leakage. Fourteen minutes post-injection (total ischemic time, 15 min), the clamp was removed. After ensuring the restoration of the blood flow, the incision was closed. To assess the effect of ischemia on renal transduction, a flank incision was made and a clamp was placed on the renal artery and vein for 15 min. Following the 15-minute ischemic time, the clamp was removed, and the vector solution was injected through the tail vein. RV and RP injections were also performed with varying durations of ischemia: <1 min (RV injection) or 0 min (RP injection), 5, 10, and 15 min. In the <1 min group, RV injection was performed with a minimal length of ischemia required for the injection. The 0 min condition was not possible for RV injection because the renal blood flow needs to be stopped when the agent is injected via RV into the kidney. RP injection was performed without the blockade of the blood flow of the renal artery and vein for the 0-min group and a clamp was placed on the ureter for 15 min regardless of the ischemic time.

Retrograde transureteral renal pelvis (RP) injection into NHPs

NHPs were managed according to the Oregon National Primate Research Center (ONPRC) program for animal care, which is fully accredited by the Association for Assessment and Accreditation of Laboratory Animal Care, International, and based on guidelines, laws, regulations and principles stated in the Animal Welfare Act (United States Department of Agriculture), Guide for the Care and Use of Laboratory Animals (Institute for Laboratory Animal Research), and the Public Health Service Policy on Humane Care and Use of Laboratory Animals (National Institutes of Health). Experimental procedures were reviewed and approved by the OHSU Institutional Biosafety Committee and the ONPRC Institutional Animal Care and Use Committee. Study animals were housed individually on a 12-h light-dark cycle in a climate-controlled, Animal Biosafety Level 2 (ABSL-2) facility that allowed protected interaction with other rhesus macaques in the same room. Seven female rhesus macaques were used for the study: one (NHP1) received the vehicle only, four (NHP2, 3, 5, 6) received AAV-KP1-CAG-tdTomoato vector, two (NHP4, 7) received AAV9-CAG-tdTomoato vector. We used female animals because the shorter urethra in females than in males would make the insertion of the fibrotic scope easier. Anti-AAV-KP1 or anti-AAV9 NAb titers were determined in the AAV vector-injected animals before the injection as described previously with minor modifications[65]. Serum samples were diluted by serial two-fold dilutions ranging from 1:5 to 1:5120. NAb titer was defined as the 50% inhibition of virus transduction calculated based on the global fitting of the data obtained from each of the serum dilutions. For the first set of the three animals (NHP2, NHP3, NHP4), we selected those that were negative (<1:5, NHP3, and NHP4) or marginally positive (1:7.5, NHP2) for NAbs. For the second set of three animals (NHP5, NHP6, and NHP7), we selected those that were unambiguously positive for NAb on purpose. Renal transduction and off-target liver transduction were assessed three weeks after injection. Serial blood and urine samples were collected to determine vector pharmacokinetics and assess the safety of the procedure. The procedure comprised the following steps: (1) Under general anesthesia, a fiber bronchoscope (11282BN1, Karl Storz) was inserted into the bladder through the urethra and the right and left ureteral orifices were identified; (2) A 0.025-inch Glidewire (Terumo) was advanced via the ureter to the right or left renal pelvis depending on the choice of the target kidney; (3) The scope was removed and a 4 French 40 cm Fogarty balloon catheter (Edwards Medical) was advanced over the wire; (4) The balloon of the Fogarty catheter was inflated at or just before the ureteropelvic junction; (5) The volume of the pelvic cavity was estimated by injecting a contrast agent under the fluoroscope; (6) The estimated pelvic volume of AAV vector solution was injected over 1 min into the pelvic cavity, followed by injection of air (~ 0.5 mL) to increase the pelvic pressure; (7) After 5 min dwelling time, the animal position was changed to the ipsilateral decubitus position so that the injected air into the renal pelvis lied over the injected AAV vector solution, and the animal was maintained in this position for an additional 5 min; (8) After a total of 10 min dwelling time, the animal position was returned to the supine position and the balloon was deflated; and (9) The balloon catheter was removed after confirming the appropriate placement of the catheter by injecting a small volume of the contrast agent.

AAV Barcode-seq analysis

Total DNA was extracted from tissues using the QIAamp MinElute Virus Spin Kit (57704, Qiagen, Venlo, Netherlands) or the KingFisher Cell and Tissue DNA Kit (97030196, Fisher Scientific, Hampton, NH) following Proteinase K (25530049, Invitrogen, Waltham, MA) treatment. Total RNA was extracted from tissues using TRIzol (15596018, Invitrogen, Waltham, MA) followed by DNase treatment using the TURBO DNA-free Kit (AM1907, Invitrogen, Waltham, MA). Point eight μg of DNase-treated RNA was reverse-transcribed with reverse transcription (RT)-specific primer (5'-GGCGGCGGTCACGAA-3') using the High-Capacity cDNA Reverse Transcription Kit (4368813, Applied Biosystems, Waltham, MA) or SuperScript IV Reverse Transcriptase (18090200, Invitrogen, Waltham, MA) in a total volume of 20 μL. One μg DNA or 4 μL

cDNA was used to PCR-amplify virus barcode (VBC) using Platinum SuperFi II DNA Polymerase (12361010, Invitrogen, Waltham, MA). Following primers were used to amplify left and right VBCs: left VBC forward (5′- FSN-SBC-ACCTACGTACTTCCGCTCAT-3′), left VBC reverse (5′-FSN-SBC-TCCCGACATCGTATTTCCGT-3′), right VBC forward (5′-FSN-SBC-ACGGAAATACGATGTCGGGA-3′) and right VBC reverse (5′-FSN-SBC-CTTCTCGTTGGGGTCTTTGC-3′). Each primer has an 8 nucleotide-long sample-specific Barcode (SBC) and a 0-4 nucleotide-long frame-shifting nucleotide (FSN) as previously described[16,63]. PCR products were mixed at an approximately equimolar ratio and sequenced at the OHSU Massively Parallel Sequencing Shared Resource (MPSSR) or Novogene (Sacramento, CA). The sequencing was performed using the following configurations on an Illumina NextSeq 500 or NovaSeq 6000 instrument: 75-cycle single-end, 150-cycle single-end, 180-cycle single-end, or 300-cycle paired-end. The quality of Illumina raw sequence reads was assessed by FastQC, in which the following four quality measures, per base sequence quality, per sequence quality scores, per base N content, and sequence length, were all met in all the data sets we used in this study. The Illumina sequencing data were then analyzed at the Pittsburgh Supercomputing Center or the Advanced Computing Center at OHSU to determine Phenotypic Difference (PD) values of each AAV capsid[16,63]. PD values indicate the 'fold change' of a phenotype compared with that of the reference control, which was AAV9 in this study. The yields of reverse-transcription (RT)-PCR products for RNA Barcode-Seq relative to the quantity of vector genomes could vary depending on the VBC sequences. This is because, as opposed to the DNA Barcode-Seq, the RNA Barcode-Seq involves additional steps, i.e., in vivo mRNA transcription and in vitro reverse transcription, in which the VBC-dependent differences cannot be canceled out by determining the ratios between input vector genome DNA read counts and vector genome transcript RNA read counts. Thus, in our RNA Barcode-Seq analysis, we introduced correction factors to normalize RNA Barcode-Seq PD values and make the PD values independent of VBC sequences. This approach helps minimize undesired variations in VBC sequence-dependent RNA Barcode-Seq readouts. The correction factor for each VBC pair in the RNA Barcode-Seq analysis was experimentally determined as follows and summarized in Supplementary Data 1. In brief, we made two AAV9-CAG-VBCx libraries that contain all the AAV-CAG-VBCx genomes packaged with the same AAV9 capsid. These two libraries were produced independently from two independent pools of all the pdsAAV-CAG-VBCx plasmids mixed at an equimolar ratio. Each of the two AAV9-CAG-VBCx virus libraries was intravenously injected into 8-week-old C57BL/6 J male mice ($n = 3$ each) to obtain an independent, duplicated set of data, each of which was obtained from 3 mice. The livers were harvested from the library-injected mice 6 weeks post-injection. Liver DNA and RNA were extracted and then subjected to the DNA and RNA Barcode-Seq analysis, which provides RNA and DNA barcode reads, respectively. The correction factors obtained by the ratio of RNA and DNA barcode reads were used to cancel out the barcode sequence-dependent differences in the in vivo mRNA transcription and the RT-PCR amplification efficiencies between VBCs. Data variations of the benchmark AAV9 capsids between biological replicates were quantified by calculating the proportion of each barcode relative to the total barcode count in the tissue of interest. While our data were normalized by the composition of the initial library, we did not perform additional adjustments by multiplying the data with vector genome per diploid genomic equivalent (vg/dge), the approach employed by Weinmann et al.[18]. Our approach is justified because our analysis focused exclusively on the relative transduction efficiencies within the kidney treated with the same procedure and did not compare transduction profiles across different organs or different procedures, making the data independent of renal transduction levels. Nonetheless, for completeness, we conducted additional adjustments on the Supplementary Fig. 1 data by vg/dge of each sample as reported by Weinmann et al.[18] and presented the results in Supplementary Fig. 11.

AAV vector genome quantification

Total DNA was extracted from tissues as described in the AAV Barcode-Seq analysis section. Blood DNA sample was prepared using the Extract-N-Amp Blood PCR Kit (XNAB2R, Sigma, St. Louis, MO) and diluted 100 times. Total DNA was extracted from 100 μL urine samples using the Wako DNA Extraction Kit (29550201, Wako Chemicals, Richmond, VA) following Proteinase K treatment. The urine DNA pellet was dissolved in 15 μL Tris-HCl buffer. AAV vector genome copy numbers were quantified by quantitative PCR (qPCR). In brief, 10–100 ng of tissue DNA or 1 μL of blood or urine DNA sample was mixed with Power SYBR Green PCR Master Mix (43-676-59, Fisher Scientific, Hampton, NH) and 25 pmol primers in a 25 μL reaction volume and subjected to qPCR using Rotor-Gene Q (Qiagen, Venlo, Netherlands). We amplified the tdTomato gene sequence and the barcode sequence for vector genome quantification using the following primers: tdTomato forward (5′-ATGGACCTGTGATGCAGAAG-3′), tdTomato reverse (5′-TTCAGCTTCAGAGCCTGGTG-3′), barcode forward (5′-ACCTACGTACTTCCGCTCAT-3′) and barcode reverse (5′-CTTCTCGTTGGGGTCTTTGC-3′). Information on copy number standards and normalization for mouse study was described previously[16]. For the NHP study, the following primers were used: *ACTB* forward (5′-AGCTGCGCCCTTTCTCACTG-3′) and *ACTB* reverse (5′-CAGAGTTC-CAAAGGAGACTC-3′). Vector genome copy numbers were expressed as double-stranded vector genome copy numbers per diploid genomic equivalent (ds-vg/dge) except in blood and urine samples, where single-stranded vector genomes per unit sample volume (vg/μL) were used for quantification and in Fig. 4a, where single-stranded vector genome copy numbers per diploid genomic equivalent (vg/dge) were presented due to the likelihood that most vector genomes in the kidneys are in single-stranded form and protected by AAV capsids 10 min post-injection. For the NHP kidneys, vector genome copy numbers were assessed in three samples obtained from the upper, middle, and lower thirds of the kidney and averaged. For the NHP livers, vector genome copy numbers of the right and left lobes were averaged.

Histological processing and analysis

Organs were harvested from mice following PBS perfusion. Harvested organs were fixed in 4% paraformaldehyde (PFA) (158127, Sigma, St. Louis, MO) and subsequently equilibrated in 30% sucrose (S5, Fisher Scientific, Hampton, NH) for cryoprotection. The fixed tissues were cryo-embedded in Tissue-Tek O.C.T. Compound (4583, Sakura Fine-tek, St. Torrance, CA), cut into 5 μm-thick sections using a cryostat, analyzed by immunofluorescence and light microscopy. Immunostaining was performed as described previously[66] using rabbit anti-WT1 (1:100, ab89901, Abcam, Cambridge, UK), rat anti-CD31 (1:100, 550274, BD Biosciences, Franklin Lakes, NJ), Lotus tetragonolobus lectin (LTL)-fluorescein (1:400, FL-1321-2, Vector Laboratories, Newark, CA), rabbit anti-HNF4α (1:200, 3113, Cell Signaling Technology, Danvers, MA), rabbit anti-NCAM1 (1:200, 99746, Cell Signaling Technology, Danvers, MA), rabbit anti-NKCC2 (1:100, SPC-401, StressMarq, Victoria, BC, Canada), rat anti-PDGFRβ (1:100, 14-1402-81, ThermoFisher Scientific, Waltham, MA), rabbit anti-AQP2 (1:100 ab199975, Abcam, Cambridge, UK), goat anti-rabbit IgG Alexa Fluor 647 (1:500, 111-605-144, Jackson ImmunoResearch, West Grove, PA), goat anti-rat IgG Alexa Fluor 647 (1:500, 112-605-167, Jackson ImmunoResearch, West Grove, PA) and Hoechst (1:10000, H3570, ThermoFisher Scientific, Waltham, MA). Immunofluorescence images were obtained using a BZ-X700 Fluorescence Microscope (Keyence, Osaka, Japan) or an LSM900 Confocal Microscope with Airyscan2 (Carl Zeiss, Oberkochen, Germany). For the quantification of tdTomato-positive proximal tubule cells, we used HNF4α instead of LTL as a proximal tubule marker because nuclear labeling by anti-HNF4α antibody enables separation of individual

proximal tubule cells in contrast to the brush border labeling by LTL, which labels proximal tubule as a segment. As shown in Supplementary Fig. 12a, anti-HNF4α antibody and LTL label the same population of cells in the kidney. We manually counted the tdTomato-positive and -negative proximal tubule cells. At least 4 images per kidney were analyzed. To determine the percentage of tdTomato-positive podocytes, five glomeruli per kidney were selected from sections that were cut in close proximity to the middle of the glomeruli. Z-stacked images were taken, and tdTomato-positive and -negative podocytes were manually counted. Representative high-magnification images used for quantification were presented in Supplementary Fig. 12 and Supplementary Movies 1–4. For the quantitative analysis of heart transduction, the heart area was determined through thresholding, and the mean fluorescent intensities (MFIs) of both the heart and the background were measured by ImageJ. The net intensity obtained by subtracting the background MFI from the heart MFI was used for the quantification of transduction. Hematoxylin and eosin (H&E) staining was also performed on NHP kidney sections to assess tissue damage.

Nanoparticle distribution in the kidney following injection
Eight-week-old C57BL/6 J male mice were injected with fluorescent polystyrene beads (G25, ThermoFisher Scientific, Waltham, MA)[67] via IV (300 μL), RV (50 μL) or RP (50 μL). The beads are fluorescent microspheres with a diameter of 25 nm, which is comparable in size to AAV. Therefore, they can be used as surrogates to investigate the distribution of AAV particles following injection. We used 4 conditions IV, RV, RP with blockade of the blood flow in the renal artery and vein, and RP without the blockade ($n = 3$ per condition). For IV injection, the distribution was assessed 30 min post-injection. For RV and RP injections, the distribution was assessed immediately after the completion of each injection procedure. Organs were harvested after PBS perfusion to remove beads from the blood vessels. Staining was performed as described above.

Assessment of albuminuria
Spot urine was collected for the quantification of albuminuria. Urine albumin concentration was measured using Albuwell M (1011, Ethos Biosciences, Logan Township, NJ) and normalized by creatinine concentration measured by Creatinine Reagent Assay (C75391250, Pointe Scientific, Canton, MI). The data was expressed as gram-per-gram creatinine (g/gCre).

Blinding
The following procedures were conducted in a blinded fashion in which the investigator remained unaware of the specifics of the vectors and samples: AAV Barcode-Seq analyses, urine albumin measurement, and a part of fluorescence microscopic studies in healthy and CKD kidneys. Although other experiments were conducted in an unblinded fashion, efforts were made to minimize bias and ensure objective observations.

Statistics
Statistical analyses were performed using GraphPad Prism 9 (version 9.5.0). Data are presented as mean ± standard error of the mean. Due to the small sample sizes in our study, normality tests such as the Shapiro-Wilk test may have limited power in detecting departures from normality. Therefore, we assumed approximate normality based on the visual inspection of the data and conducted parametric tests, the results of which are presented in this paper. In this approach, comparisons between two groups were performed using a two-tailed Welch's t test. For data sets with more than two groups, significance was determined by a one-way ANOVA or two-way ANOVA followed by Tukey's post hoc test or a two-tailed Welch's t test with Bonferroni correction. $P < 0.05$ was considered statistically significant.

Reporting summary
Further information on research design is available in the Nature Portfolio Reporting Summary linked to this article.

Data availability
The NGS data generated in this study have been deposited in the Sequence Read Archive under accession code PRJNA998389 [http://www.ncbi.nlm.nih.gov/bioproject/998389]. The NGS read count data are available on Zenodo [https://doi.org/10.5281/zenodo.14053051]. The data generated and used in the figures are provided in the Source Data file. Source data are provided in this paper.

Code availability
The scripts and sample data used for the Barcode-Seq analysis are available on both GitHub [https://github.com/nakaih-ohsu/AAV_Kidney_2023.git] and Zenodo [https://doi.org/10.5281/zenodo.14037951].

References
1. Li, C. & Samulski, R. J. Engineering adeno-associated virus vectors for gene therapy. *Nat. Rev. Genet.* **21**, 255–272 (2020).
2. Wang, J. H., Gessler, D. J., Zhan, W., Gallagher, T. L. & Gao, G. Adeno-associated virus as a delivery vector for gene therapy of human diseases. *Signal Transduct. Target Ther.* **9**, 78 (2024).
3. Groopman, E. E. et al. Diagnostic utility of exome sequencing for kidney disease. *N. Engl. J. Med.* **380** 142–151 (2019).
4. Lata, S. et al. Whole-exome sequencing in adults with chronic kidney disease: A pilot study. *Ann. Intern Med.* **168** 100–109 (2018).
5. Hildebrandt, F. Genetic kidney diseases. *Lancet* **375**, 1287–1295 (2010).
6. Ikeda, Y., Sun, Z., Ru, X., Vandenberghe, L. H. & Humphreys, B. D. Efficient gene transfer to kidney mesenchymal cells using a synthetic adeno-associated viral vector. *J. Am. Soc. Nephrol.* **29**, 2287–2297 (2018).
7. Lang, J. F., Toulmin, S. A., Brida, K. L., Eisenlohr, L. C. & Davidson, B. L. Standard screening methods underreport AAV-mediated transduction and gene editing. *Nat. Commun.* **10**, 3415 (2019).
8. Ding, W. Y. et al. Adeno-associated virus gene therapy prevents progression of kidney disease in genetic models of nephrotic syndrome. *Sci. Transl. Med.* **15**, eabc8226 (2023).
9. Wu, G. et al. Adeno-associated virus-based gene therapy treats inflammatory kidney disease in mice. *J. Clin. Invest.* **134**, e174722 (2024).
10. Rocca, C. J., Ur, S. N., Harrison, F. & Cherqui, S. rAAV9 combined with renal vein injection is optimal for kidney-targeted gene delivery: conclusion of a comparative study. *Gene Ther.* **21**, 618–628 (2014).
11. Rubin, J. D., Nguyen, T. V., Allen, K. L., Ayasoufi, K. & Barry, M. A. Comparison of gene delivery to the kidney by adenovirus, adeno-associated virus, and lentiviral vectors after intravenous and direct kidney injections. *Hum. Gene Ther.* **30**, 1559–1571 (2019).
12. Saito, S. et al. rAAV6-mediated miR-29b delivery suppresses renal fibrosis. *Clin. Exp. Nephrol.* **23**, 1345–1356 (2019).
13. Asico, L. D. et al. Nephron segment-specific gene expression using AAV vectors. *Biochem. Biophys. Res. Commun.* **497**, 19–24 (2018).
14. Konkalmatt, P. R. et al. Renal rescue of dopamine D2 receptor function reverses renal injury and high blood pressure. *JCI Insight* **1**, e85888 (2016).
15. Colella, P., Ronzitti, G. & Mingozzi, F. Emerging issues in AAV-mediated in vivo gene therapy. *Mol. Ther. Methods Clin. Dev.* **8**, 87–104 (2018).
16. Adachi, K., Enoki, T., Kawano, Y., Veraz, M. & Nakai, H. Drawing a high-resolution functional map of adeno-associated virus capsid by massively parallel sequencing. *Nat. Commun.* **5**, 3075 (2014).

17. Pekrun, K. et al. Using a barcoded AAV capsid library to select for clinically relevant gene therapy vectors. *JCI Insight* **4**, e131610 (2019).

18. Weinmann, J. et al. Identification of a myotropic AAV by massively parallel in vivo evaluation of barcoded capsid variants. *Nat. Commun.* **11**, 5432 (2020).

19. Grimm, D. et al. In vitro and in vivo gene therapy vector evolution via multispecies interbreeding and retargeting of adeno-associated viruses. *J. Virol.* **82**, 5887–5911 (2008).

20. Shen, S. et al. Engraftment of a galactose receptor footprint onto adeno-associated viral capsids improves transduction efficiency. *J. Biol. Chem.* **288**, 28814–28823 (2013).

21. Dalkara, D. et al. In vivo-directed evolution of a new adeno-associated virus for therapeutic outer retinal gene delivery from the vitreous. *Sci. Transl. Med.* **5**, 189ra176 (2013).

22. Kotchey, N. M. et al. A potential role of distinctively delayed blood clearance of recombinant adeno-associated virus serotype 9 in robust cardiac transduction. *Mol. Ther.* **19**, 1079–1089 (2011).

23. Satchell, S. C. & Braet, F. Glomerular endothelial cell fenestrations: an integral component of the glomerular filtration barrier. *Am. J. Physiol. Ren. Physiol.* **296**, F947–F956 (2009).

24. Latta, H. An approach to the structure and function of the glomerular mesangium. *J. Am. Soc. Nephrol.* **2**, S65–S73 (1992).

25. Sakai, T. & Kriz, W. The structural relationship between mesangial cells and basement membrane of the renal glomerulus. *Anat. Embryol.* **176**, 373–386 (1987).

26. Choi, C. H., Zuckerman, J. E., Webster, P. & Davis, M. E. Targeting kidney mesangium by nanoparticles of defined size. *Proc. Natl. Acad. Sci. USA* **108**, 6656–6661 (2011).

27. Guo, L. et al. Targeted delivery of celastrol to mesangial cells is effective against mesangioproliferative glomerulonephritis. *Nat. Commun.* **8**, 878 (2017).

28. Rheault, M. N. et al. Mouse model of X-linked Alport syndrome. *J. Am. Soc. Nephrol.* **15**, 1466–1474 (2004).

29. Yu, A. S. L. et al. *Brenner & Rector's the Kidney* (Elsevier, Philadelphia, PA, 2020).

30. Jankowski, J., Floege, J., Fliser, D., Bohm, M. & Marx, N. Cardiovascular disease in chronic kidney disease: Pathophysiological insights and therapeutic options. *Circulation* **143**, 1157–1172 (2021).

31. Touchberry, C. D. et al. FGF23 is a novel regulator of intracellular calcium and cardiac contractility in addition to cardiac hypertrophy. *Am. J. Physiol. Endocrinol. Metab.* **304**, E863–E873 (2013).

32. Neuburg, S. et al. Genetic background influences cardiac phenotype in murine chronic kidney disease. *Nephrol. Dial. Transpl.* **33**, 1129–1137 (2018).

33. Amann, K. et al. Reduced capillary density in the myocardium of uremic rats-a stereological study. *Kidney Int.* **42**, 1079–1085 (1992).

34. Scallan, C. D. et al. Human immunoglobulin inhibits liver transduction by AAV vectors at low AAV2 neutralizing titers in SCID mice. *Blood* **107**, 1810–1817 (2006).

35. Gray, S. J. et al. Preclinical differences of intravascular AAV9 delivery to neurons and glia: a comparative study of adult mice and nonhuman primates. *Mol. Ther.* **19**, 1058–1069 (2011).

36. Begley, D. J., Pontikis, C. C. & Scarpa, M. Lysosomal storage diseases and the blood-brain barrier. *Curr. Pharm. Des.* **14**, 1566–1580 (2008).

37. Gray, S. J., Nagabhushan Kalburgi, S., McCown, T. J. & Jude Samulski, R. Global CNS gene delivery and evasion of anti-AAV-neutralizing antibodies by intrathecal AAV administration in non-human primates. *Gene Ther.* **20**, 450–459 (2013).

38. Burdon, D. W. Immunoglobulins of normal human urine and urethral secretions. *Immunology* **21**, 363–368 (1971).

39. Chung, D. C. et al. Adeno-associated virus-mediated gene transfer to renal tubule cells via a retrograde ureteral approach. *Nephron Extra* **1**, 217–223 (2011).

40. Shen, X. et al. Transparenchymal renal pelvis injection of recombinant adeno-associated virus serotype 9 vectors is a practical approach for gene delivery in the kidney. *Hum. Gene Ther. Methods* **29**, 251–258 (2018).

41. Clark, J. Z. et al. Representation and relative abundance of cell-type selective markers in whole-kidney RNA-Seq data. *Kidney Int.* **95**, 787–796 (2019).

42. Chevalier, R. L. The proximal tubule is the primary target of injury and progression of kidney disease: role of the glomerulotubular junction. *Am. J. Physiol. Ren. Physiol.* **311**, F145–F161 (2016).

43. Meyer, K. et al. Improving single injection CSF delivery of AAV9-mediated gene therapy for SMA: a dose-response study in mice and nonhuman primates. *Mol. Ther.* **23**, 477–487 (2015).

44. Quirin, K. A. et al. Safety and efficacy of AAV retrograde pancreatic ductal gene delivery in normal and pancreatic cancer mice. *Mol. Ther. Methods Clin. Dev.* **8**, 8–20 (2018).

45. Shen, W., Liu, S. & Ou, L. rAAV immunogenicity, toxicity, and durability in 255 clinical trials: A meta-analysis. *Front. Immunol.* **13**, 1001263 (2022).

46. Schievenbusch, S. et al. Combined paracrine and endocrine AAV9 mediated expression of hepatocyte growth factor for the treatment of renal fibrosis. *Mol. Ther.* **18**, 1302–1309 (2010).

47. Kopp, J. B. et al. Podocytopathies. *Nat. Rev. Dis. Prim.* **6**, 68 (2020).

48. Babickova, J. et al. Regardless of etiology, progressive renal disease causes ultrastructural and functional alterations of peritubular capillaries. *Kidney Int.* **91**, 70–85 (2017).

49. Horiuchi, M. et al. Intravenous immunoglobulin prevents peripheral liver transduction of intrathecally delivered AAV vectors. *Mol. Ther. Methods Clin. Dev.* **27**, 272–280 (2022).

50. Kruzik, A. et al. Prevalence of anti-adeno-associated virus immune responses in international cohorts of healthy donors. *Mol. Ther. Methods Clin. Dev.* **14**, 126–133 (2019).

51. Tse, L. V. et al. Structure-guided evolution of antigenically distinct adeno-associated virus variants for immune evasion. *Proc. Natl. Acad. Sci. USA* **114**, E4812–E4821 (2017).

52. Meliani, A. et al. Antigen-selective modulation of AAV immunogenicity with tolerogenic rapamycin nanoparticles enables successful vector re-administration. *Nat. Commun.* **9**, 4098 (2018).

53. Salas, D. et al. Immunoadsorption enables successful rAAV5-mediated repeated hepatic gene delivery in nonhuman primates. *Blood Adv.* **3**, 2632–2641 (2019).

54. Leborgne, C. et al. IgG-cleaving endopeptidase enables in vivo gene therapy in the presence of anti-AAV neutralizing antibodies. *Nat. Med.* **26**, 1096–1101 (2020).

55. Elmore, Z. C., Oh, D. K., Simon, K. E., Fanous, M. M. & Asokan, A. Rescuing AAV gene transfer from neutralizing antibodies with an IgG-degrading enzyme. *JCI Insight* **5**, e139881 (2020).

56. Cai, A., Chatziantoniou, C. & Calmont, A. Vascular permeability: Regulation pathways and role in kidney diseases. *Nephron* **145**, 297–310 (2021).

57. Dong, K. et al. Renal plasticity revealed through reversal of polycystic kidney disease in mice. *Nat. Genet.* **53**, 1649–1663 (2021).

58. Lin, X., Suh, J. H., Go, G. & Miner, J. H. Feasibility of repairing glomerular basement membrane defects in Alport syndrome. *J. Am. Soc. Nephrol.* **25**, 687–692 (2014).

59. Tasfaout, H. et al. Split intein-mediated protein trans-splicing to express large dystrophins. *Nature* **632**, 192–200 (2024).

60. Pasi, K. J. et al. Multiyear Follow-up of AAV5-hFVIII-SQ Gene Therapy for Hemophilia A. *N. Engl. J. Med.* **382**, 29–40 (2020).

61. Mendell, J. R. et al. Assessment of systemic delivery of rAAVrh74.MHCK7.micro-dystrophin in children with duchenne muscular dystrophy: A nonrandomized controlled trial. *JAMA Neurol.* **77**, 1122–1131 (2020).

62. Pierce, E. A. et al. Gene editing for CEP290-associated retinal degeneration. *N. Engl. J. Med.* **390**, 1972–1984 (2024).

63. Earley, L. F. et al. Adeno-associated Virus (AAV) assembly-activating protein is not an essential requirement for capsid assembly of AAV serotypes 4, 5, and 11. *J. Virol.* **91**, e01980–16 (2017).
64. Woodard, L. E. et al. Hydrodynamic renal pelvis injection for non-viral expression of proteins in the kidney. *J. Vis. Exp.* **131**, 56324 (2018).
65. Adachi, K. et al. Adeno-associated virus-binding antibodies detected in cats living in the Northeastern United States lack neutralizing activity. *Sci. Rep.* **10**, 10073 (2020).
66. Furusho, T. et al. Renal TNFα activates the WNK phosphorylation cascade and contributes to salt-sensitive hypertension in chronic kidney disease. *Kidney Int.* **97**, 713–727 (2020).
67. Smith, R. O. et al. Vascular permeability in retinopathy is regulated by VEGFR2 Y949 signaling to VE-cadherin. *Elife* **9**, e54056 (2020).

Author contributions

T.F. and H.N. designed the study and wrote the manuscript. K.A. produced the AAV library and characterized AAV vectors following intravenous administration. T.F., M.G.L., R.D., H.H., and S.L. performed fluorescence microscopy analysis. T.F. and M.G.L. performed urine albumin ELISA. T.F. and P.R. quantified the vector genome copy numbers. T.F. and R.D. performed the study of microsphere distribution. T.F., M.G.L., and L.L. performed ELISA for anti-AAV binding antibodies to screen NHPs. H.H. performed a pharmacokinetic study of NHPs. K.Y. and M.H. performed transcatheter retrograde renal pelvis injections in NHPs. G.A.D. coordinated and managed the NHP studies and directed the performance of the neutralizing antibody assays for NHPs. H.N. developed the algorithm for data analysis and wrote the computer scripts. A.S. produced the AAV vectors expressing a marker gene and assisted the histological analysis. Other experiments were performed by T.F. N.A. did the pathological assessment of the NHP sample. All authors read and approved the final version of the paper.

Competing interests

K.A. and H.N. receive a royalty of AAV-related technologies licensed by Takara Bio Inc. and Capsigen Inc. H.N. serves as a consultant for biotech companies, is a co-founder of Capsigen Inc., and holds shares of Capsigen Inc. and Sphere Gene Therapeutics. The remaining authors declare no competing interests.

Additional information

Supplementary information The online version contains supplementary material available at https://doi.org/10.1038/s41467-024-54475-9.

Correspondence and requests for materials should be addressed to Hiroyuki Nakai.

Peer review information *Nature Communications* thanks Mark Kay, Arun Srivastava, and the other anonymous reviewer(s) for their contribution to the peer review of this work. A peer review file is available.

Reprints and permissions information is available at http://www.nature.com/reprints

Publisher's note Springer Nature remains neutral with regard to jurisdictional claims in published maps and institutional affiliations.